Climate Dynamics (2024) 62:5351–5371
https://doi.org/10.1007/s00382-024-07166-6

ORIGINAL ARTICLE

Enhancing spatiotemporal paleoclimate reconstructions of hydroclimate across the Mediterranean over the last millennium

Kevin J. Anchukaitis[1] · Ramzi Touchan[2] · David M. Meko[2] · Dalila Kherchouche[3] · Said Slimani[4] · Fatih Sivrikaya[5] · Rachid Ilmen[6] · Ioannis Mitsopoulos[7] · Jean Stephan[8] · Jihad Attieh[9] · Foued Hasnaoui[10] · J. Julio Camarero[11] · Raúl Sánchez-Salguero[11,12] · Frederic Guibal[13] · Alma Piermattei[14,18] · Andreas Christou[15] · Jordan Krcmaric[16] · Benjamin I. Cook[17]

Received: 16 March 2023 / Accepted: 15 February 2024 / Published online: 27 March 2024

Abstract
The Mediterranean region is projected to experience severe drying trends and more extreme hydroclimate events as a consequence of anthropogenic climate change over the next century. In some places this signal may have already emerged from natural variability, but uncertainty in long-term paleoclimate reconstructions can be a significant challenge to the detection of the influence of rising CO_2 on droughts. Here we provide expanded context for recent and future hydroclimate changes with a new high-resolution (0.5^o) spatial reconstruction of the Palmer Drought Severity Index (PDSI) using a tree-ring network that spans much of the last millennium. This network provides new perspective on the existing Old World Drought Atlas (OWDA) and allows us to characterize differences between OWDA and our reconstruction. In light of the uncertainties we identify, we also reexamine previous conclusions about the severity of recent droughts in the context of earlier centuries. We find that, in both the western Mediterranean and the Levant, recent dry periods remain the worst in at least the last 500 years, but our assessment of the significance and confidence in this finding is affected by differences in the tree-ring networks used for the reconstructions. Long millennium-length hydroclimate reconstructions in the Mediterranean do provide the opportunity to understand variability and trends in the hydroclimate of the region, but extant uncertainties arising from the existing tree-ring chronology network and methodological choices call attention to locations that require further proxy collection, chronology updates, and statistical scrutiny.

Keywords Drought · Megadrought · Dendrochronology · Uncertainty · Hydroclimate · Mediterranean

1 Introduction

Ongoing and future climate change is a global phenomenon, but it is projected to have a disproportionate impact on certain regions of the world, in particular the Mediterranean (Allen and Ingram 2002; Giorgi 2006; Christensen et al. 2007; García-Ruiz et al. 2011; Kelley et al. 2012a; Tuel and Eltahir 2020; Tramblay et al. 2020; Cook et al. 2020a; Douville et al. 2021; Cos et al. 2022). The region is projected to experience reductions in rainfall in all seasons that will be further exacerbated by the effects of higher temperatures on drought severity (García-Ruiz et al. 2011; Cook et al. 2014; Vicente-Serrano et al. 2014; Tramblay et al. 2020; Vicente-Serrano et al. 2020; Cook et al. 2020a). The risk of a severe megadrought event also increases in the future (Cook et al. 2020a; Stevenson et al. 2022). In some parts of the region the signal of anthropogenic influence on precipitation and drought may already be emerging from natural variability (Touchan et al. 2011; Kelley et al. 2012a, 2015; Cook et al. 2016; Seager et al. 2019).

However, the importance of internal variability at interannual to decadal scales, climate model limitations in simulating the complete range of precipitation processes, and the influence of various large-scale ocean–atmosphere dynamics all affect the robust detection and attribution of trends in Mediterranean drought (Altava-Ortiz et al. 2011; Kelley et al. 2012b; Barkhordarian et al. 2013; Mariotti et al. 2015; Anchukaitis et al. 2019; Seager et al. 2020; Suárez-Moreno et al. 2022). For instance, Kelley et al. (2012a) identified important differences between climate model simulations and the observed patterns of drying in the Mediterranean over the late 20th century, particularly in winter, a

Extended author information available on the last page of the article

discrepancy that Kelley et al. (2012b) subsequently linked to the importance of internal climate variability. Observed drought patterns reflect a combination of the unforced internal variability and the forced response of the hydroclimate system (Cook et al. 2011; Suárez-Moreno et al. 2022). Mariotti et al. (2015) concluded that the signal of forced changes in precipitation in the region would emerge later in the century due to the influence of large internal climate system variability.

Characterizing internal variability in hydroclimate is therefore of critical importance for detecting the signal of forced changes in precipitation across the Mediterranean. However, the instrumental record provides limited opportunities to do so, particularly at the decadal and multidecadal time scales relevant to attributing the recent sustained drought events and observed regional trends toward drier conditions. Even in the Mediterranean Basin where there is a relatively large amount of available meteorological data, reliable weather observations in parts of the region are sparse prior to the 1940 s (c.f. Touchan and Hughes 1999; Zhang et al. 2005). Tree-ring paleoclimate data, however, provide a way to effectively extend the observations of rainfall and soil moisture variability over the past millennium and to better characterize the range of internal variability (c.f. Cook et al. 2010b, 2018, 2022).

The Mediterranean Basin has increasingly been the focus of tree-ring reconstructions of past hydroclimate variability, given the importance of precipitation variability for human society in the region and the anticipated trend toward drier conditions (Chenoweth et al. 2011; Lelieveld et al. 2012; Holmgren et al. 2016; Xoplaki et al. 2018; Cramer et al. 2018). A number of studies have focused on local and regional reconstructions of hydroclimate using a range of species (e.g. Touchan et al. 1999a, 2003, 2005b, a; Griggs et al. 2007; Touchan et al. 2007; Esper et al. 2007; Touchan et al. 2008a, b; Akkemik et al. 2008; Nicault et al. 2008; Köse et al. 2011; Heinrich et al. 2013; Martin-Benito et al. 2016; Tejedor et al. 2016, 2017; Klippel et al. 2018; Esper et al. 2021). A growing network of tree-ring sites across the region has also allowed for spatial field reconstructions. For instance, Nicault et al. (2008) used an artificial neural network on a network of tree-ring sites to perform a non-linear reconstruction of a 2.5×2.5 degree gridded (April to September) drought field. Touchan et al. (2011) reconstructed the spatial pattern of May through August Palmer Drought Severity Index (PDSI) over most of the last millennium in northwestern Africa. More recently, Cook et al. (2015) created the 'Old World Drought Atlas' (OWDA) which included the Mediterranean region. Rao et al. (2017) and Anchukaitis et al. (2019) used the OWDA to study forced and unforced climate variability over the region. Cook et al. (2019) used the tree-ring network from the OWDA to reconstruct the North Atlantic Oscillation over the last millennium. Finally, Cook et al. (2016) used the OWDA to characterize drought variability over much of the last millennium over the region, identifying robust spatiotemporal features of the reconstruction and identifying recent drought in the Levant region as exceptional in the context of the last 900 years.

The OWDA tree-ring network is comprised primarily of long tree-ring chronologies that span at least the last millennium. Because of this focus, the OWDA's proxy network consists of only 42 chronologies from the Mediterranean Basin (30 to 46N, 10W to 46E). However, a substantial number of additional chronologies are also available from the region or have been developed since the OWDA was published. New chronologies from northwest Africa as well as a dense network of chronologies from Anatolia and the eastern Mediterranean allow us to evaluate the influence of additional tree-ring chronologies on reconstructions of past drought in the region, particularly in areas where the number of chronologies is sparse. Because the OWDA also required that a minimum of 20 tree-ring chronologies be available for each reconstructed grid point in the atlas, in many locations the OWDA uses chronologies from more than a 1000 km away from the target grid point, including tree-ring chronologies from western and central Europe. While Cook et al. (2015) showed that there is large-scale covariance of hydroclimate across Europe and the Mediterranean that in some cases permits such a large predictor domain (see their Fig. S5), this comes with the risk that more localized variability may be subsumed in this continental-scale focus. Cook et al. (2015) found an average *e*-folding distance near 800 km across the entire OWDA region, but this was shorter in the Mediterranean. The addition of new tree-ring chronologies to large-scale reconstructions like the OWDA could therefore help improve the local and regional characterization of drought duration and severity and help refine estimates of reconstruction uncertainty.

Here we use a larger network of tree-ring chronologies from across the Mediterranean region to create and evaluate a new high-resolution spatiotemporal reconstruction of drought over much of the the last millennium. Specifically, we examine how inferences about past and current drought severity are sensitive to our reconstruction choices and the inclusion of a larger number of tree-ring predictors with varying seasonal sensitivity to precipitation. We also compare our new hydroclimate reconstruction to OWDA in order to identify regions of agreement and disagreement. Based on our reconstruction, we identify regions and likely sources of uncertainty when using paleoclimate information for the assessment of recent soil moisture trends.

2 Materials and methods

2.1 Tree-ring chronologies

Our complete tree-ring chronology network consists of 165 sites from across the Mediterranean region (bounded herein by 30 to 46N, and 10E to 46W), including Turkey, Syria, Lebanon, Cyprus, Greece, Morocco, Algeria, Tunisia, southeastern Spain, Corsica, and southern Italy (Fig. 1). The lengths of the chronologies range from the shortest at 80 years (at Tekrouna in Tunisia) to the longest currently at 1129 years (Col de Zad, Morocco) (Fig. 1). A similar spread of ages is present if the eastern Mediterranean is considered alone. All chronologies were developed following standard dendrochronological methods (Stokes and Smiley 1968; Fritts 1976; Cook and Kairiūkštis 1990) and are more fully described in Touchan et al. (2014a) and Touchan et al. (2017). A uniform standardization procedure was applied for chronology development, with each individual series of tree-ring width measurements at each site fit with a cubic smoothing spline with a 50% frequency response at 67% of the series length to remove non-climatic trends due primarily to age and tree geometry (Cook and Briffa 1990). The detrended series were modeled with a low-order autoregressive model to remove persistence not related to climatic variations. The individual tree indices were combined into a single master chronology for each site using a bi-weight robust estimate of the mean (Cook 1985). For site-by-site statistical comparisons between tree-ring and climate data, both the chronologies and local precipitation or PDSI time series were first-differenced to minimize the influence of any trends on the correlation. The ARSTAN chronologies were used for the spatial PDSI reconstruction in order to retain the portion of autocorrelation in the chronologies that is potentially related to climate (Cook 1985).

2.2 Climate data

For our regional climate target, we use the 0.5° self-calibrating Palmer Drought Severity Index (PDSI) from Barichivich et al. (2020) which is updated from van der Schrier et al. (2013) through 2019 using the high resolution CRU TS 4.04 climate dataset (Harris et al. 2020). The PDSI is a dimensionless metric that integrates the influence of precipitation amount, evapotranspiration, and persistence in order to quantify local variability in soil moisture (Palmer 1965; van der Schrier et al. 2013; Wells et al. 2004). Locally the metric is centered near zero (indicating normal soil moisture conditions) and normalized, allowing comparisons of relative anomalies across regions with different hydroclimate regimes. Recent versions of the PDSI, including Barichivich et al. (2020), use the Penman-Monteith equation to approximate evapotranspiration. Average summer (typically June through August) PDSI integrates precipitation and temperature over the prior water year, including the winter Mediterranean wet season, and therefore provides a uniform reconstruction target that reflects an integrated moisture signal (Cook et al. 1999). However, varying seasonal precipitation response in trees across our network is expected to make some chronologies better predictors of summer PDSI than others (e.g. Meko et al. 1993). In order to identify differential seasonal responses to precipitation across our network, we also correlated each chronology against the closest grid point in the CRU TS4.04 gridded precipitation dataset

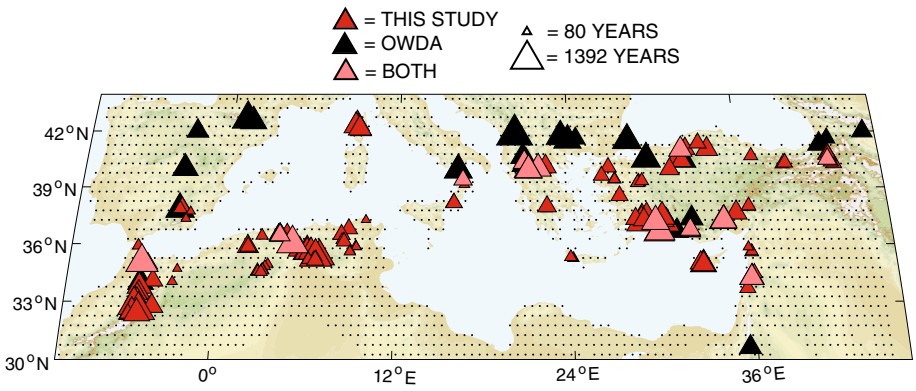

Fig. 1 Tree-ring chronologies used in this study (red triangles), those used in the OWDA (black triangles, Cook et al. (2015)), and sites which are present in both studies. However, while the same or similar locations might be used in both studies, the detrending and standardization differ between them. The size of the symbol corresponds with the length of the chronology. Black dots show the grid center of the target (predictand) PDSI field (Barichivich et al. 2020). Full details for these chronologies are in Touchan et al. (2014a) and Touchan et al. (2017). Chronology location and species for Cook et al. (2015) is present in their supplemental material. Chronologies from our network that do not extend back to 1900 CE were excluded from the reconstruction (see Materials and methods)

(Harris et al. 2020) and assessed the association with prior winter, spring, and early summer rainfall. Finally, we evaluated the optimal season for our PDSI reconstruction based on the correlation between each chronology and its local monthly and seasonal PDSI data.

2.3 Reconstruction method

We use the Point-by-Point Regression (PPR) method (Cook et al. 1999) to reconstruct past PDSI values in space and time across the Mediterranean (30 to 46N, and 10E to 46W). This region overlaps with the southern portion of the larger spatial domain of the OWDA. PPR has been extensively applied to PDSI reconstructions (Cook et al. 2004, 2010a; Touchan et al. 2011; Cook et al. 2015; Palmer et al. 2015; Williams et al. 2020; Cook et al. 2020b) as well as temperature reconstructions (Cook et al. 2013; Anchukaitis et al. 2017) using networks of climate-sensitive tree-ring chronologies. PPR is a nested iterative 'region-of-interest' procedure that calibrates and validates a multivariate principal component regression (PCR) model individually at each point in a gridded target observational field using the available tree-ring chronologies within a certain radius of that grid point as the possible predictors. At each point, the tree-ring chronologies within a given radius are first identified and screened for correlation with the PDSI series at the target grid point. Here, as in Cook et al. (1999), we retain any tree-ring chronology that correlated at $p < 0.10$ with the predictand. The principal components (PCs) of these predictor tree-ring chronologies are calculated from their normalized [0,1] time series. We retain all PCs with an eigenvalue greater than 1 (Kaiser 1960; Cook et al. 1999) as potential predictors in a stepwise multiple linear regression. The regression model is calibrated over a portion of the overlapping period with the available gridded observational data. Our domain contains 2181 grid points with instrumental PDSI data (Fig. 1, Barichivich et al. (2020)).

We require that all chronologies extend back at least until 1900 CE and forward to at least 2000 in order to be considered predictors for PPR, which eliminates the shortest chronologies from our predictor network (Touchan et al. 2014a, 2017) as well as some sites collected prior to 2000 but not since updated (Touchan and Hughes 1999; Touchan et al. 2014c; Cook et al. 2015) leaving 156 chronologies available for the field reconstruction. We use a split sample calibration and validation procedure (Snee 1977) with two periods: 1940 to 1969 and 1970 to 2000. These periods reflect a trade-off between the reliability of the available observational climate data and the overlapping span of the chronologies (Zhang et al. 2005; Kuglitsch et al. 2009; Tanarhte et al. 2012; Beguería et al. 2016). We validate the model by performing both an early calibration and late calibration and assessing the model's accuracy and skill on the data from the withheld period. The final reconstruction is based on a calibration model utilizing all of the available years. We use a nested approach such that for each change in sample size (as shorter tree-ring chronologies become unavailable) we recalculate the regression model and assess its accuracy and skill with the reduced number of predictors (Meko 1997). The possible tree-ring reconstruction period considered here is 1200 to 2000 CE, which we then extend forward (c.f. Cook et al. 2004, 2010a; Griffin and Anchukaitis 2014; Cook et al. 2015; Williams et al. 2020) to 2019 using the observational gridded data (Barichivich et al. 2020). We observe that in northwestern Africa it is possible to extend locally skillful reconstructions back into the first millennium (Touchan et al. 2008a, 2011). Nevertheless, the declining sample size by 1200 CE means that many regions are without sufficient tree-ring data prior to that point in time for the search radius and spatial domain of the tree-ring network used here. Similarly, although some tree-ring chronologies do extend further into the 21st century, sample size across our study region declines very rapidly in the early 2000s (Touchan et al. 2014a, 2017).

Following Williams et al. (2020) and Williams et al. (2021), we also use an ensemble of search radii between 400 and 1000 km at 100 km intervals. There is no single definitive way to select a search radius to use in PPR, although the choice is typically guided by the spatial decorrelation of the target climate field (e.g. Cook et al. 1999, 2010a, 2013, 2015; Anchukaitis et al. 2017; Williams et al. 2020). The use of an ensemble of search radii here allows us to examine the impact of that choice on both the spatial skill of the reconstruction (Williams et al. 2020) and on the similarity of our reconstruction and the OWDA, which used search radii larger than 1500 km in some cases. In our subsequent analyses we consider both the individual ensemble members as well as the ensemble mean.

2.4 Statistical analyses

We conducted several analyses of our new spatial PDSI reconstruction, including comparisons with the OWDA. In order to evaluate the structure and robustness of large-scale patterns in our reconstruction in space and time, we calculated the leading principal components (PCs) of the reconstructed field and compared these with the original target field and its respective leading principal components. Due to the decline in skillfully reconstructed grid points earlier than 1300, we restricted the PC calculation for the reconstruction to the period from 1300 to 2000, although again it is possible to use longer periods in northwestern Africa where skill remains robust through the earlier period.

In order to evaluate how our reconstruction compares with the OWDA, we correlated the leading PCs of our reconstruction against the OWDA. We also calculated the

pointwise correlation between the two reconstructed fields. These analyses allow us to identify regions where our reconstruction and the OWDA agree and where the differences in the underlying tree-ring data and methodological choices lead to uncertainties in past PDSI values.

Following Cook et al. (2016), we identified recent (late 20th and early 21st century) periods of persistent severe drought in both the western Mediterranean (Morocco, Algeria, Tunisia, Spain, and Portugal: 32–42N, 10W to 0E) and the eastern Mediterranean ('the Levant': 30–37N, 33 to 40E). We then calculated the mean PDSI for moving windows of the same length in each regional time series. Cook et al. (2016) determined the start and end of these periods based on a 10 year loess smooth. With the additional years present in our PDSI dataset (Barichivich et al. 2020), we extend the end date of some of these events further forward in time. In order to quantify the natural range of dry and wet anomalies on these time scales, we calculated the interquartile range (IQR) of these moving-window mean PDSI values. We also identified the driest period of the same length prior to the most recent drought. We applied a t-test to the PDSI values for both the most recent and prior events as a parametric test for differences between the mean of the years comprising the two events. We additionally estimated uncertainties using a non-parametric bootstrap resampling procedure where we randomly draw years from each window with replacement, recalculating the mean PDSI for these intervals 10,000 times and using these to bootstrap confidence limits around each event mean value as well as quantifying for what percent of these paired iterations the recent drought remains drier than the prior event.

3 Results

3.1 Climate signal

Site-by-site correlations with summer (JJA) PDSI (Fig. 2A) show a variable association across the Mediterranean domain . In Morocco, Algeria, Tunisia, and parts of Turkey, correlations between tree-ring chronologies and local JJA PDSI are particularly strong ($r > 0.50$) and significant at ($p << 0.05$, c.f. Esper et al. 2007; Touchan et al. 2008a, 2011, 2017). A strong summer PDSI signal is linked to a strong prior winter and spring precipitation signal in these chronologies (Fig. 2B). However, in southeastern Spain, southern Italy, Greece, and the Levant the local summer PDSI correlations are comparatively weak ($r = 0.20$ to $r = 0.40$). In Greece and Turkey, the association with PDSI is also more heterogeneous than in northwest Africa, likely due to the weaker connection between the dominant late Spring precipitation signal in these chronologies (Fig. 2C; Touchan et al. 2014a, c) and summer PDSI. Figure 3 shows that the pairwise correlations between prior winter through current spring (October-June) total rainfall and summer PDSI are substantially stronger for the majority of our domain compared with the local correlations between JJA PDSI and total May-June precipitation, which is very likely one of the primary factors in the varying PDSI signal across the tree-ring network. Over the entire study region, we found that differences in the strength of the climate association using a JJA PDSI season or a longer MJJA season are minimal and appear random across the network of sites. In North America, Cook et al. (1999) used the JJA PDSI for drought reconstruction because it was able to integrate the various seasonal precipitation responses in the network and provided a uniform predictand target over the full spatial domain. We have previously followed a similar strategy in the region (Touchan et al. 2011). This practice necessarily reflects a trade-off between the various signals present in a diverse large-scale network of tree-ring proxy data and the interpretive value of a single consistent climate target field.

3.2 Reconstruction skill and accuracy

Despite the spatially-varying association with hydroclimate described above, our ensemble mean reconstruction of JJA PDSI demonstrates skill across a large portion of the region (Fig. 4). For the best replicated reconstruction nest and using a late calibration period and early validation period, we observe high calibration and validation R^2 values across all of northwestern Africa, southern Spain, much of Turkey and into the Balkans, and substantial parts of the Levant. Overall for this period there is similarly significant skill in the Reduction of Error (RE) and Coefficient of Efficiency (CE), with scores above zero for 96% and 77% of the domain, respectively. RE and CE scores are particularly high over northwestern Africa and southern Spain, northern and western Turkey, and parts of the Balkans, but remain greater than zero even in much of the Levant. Similar, although slightly weaker, accuracy and skill scores are observed when using an early calibration and late validation period.

We can also evaluate the accuracy and skill of the ensemble mean reconstruction as we progress back in time using our nested split sample reconstruction procedure (Figs. 5 and 6). Because the reconstruction at each grid point is calibrated and validated anew each time there is a change in the available tree-ring chronologies back in time, we can evaluate the accuracy and skill for periods in the past when the predictor network was reduced compared to the more recent period. In other words, although we cannot know how well a reconstruction reproduces the pre-instrumental period, we can quantify how well the reduced network of tree-ring predictors during that period calibrates and validates against the modern observations. Once again, for a late calibration and early validation period, we observe consistently high

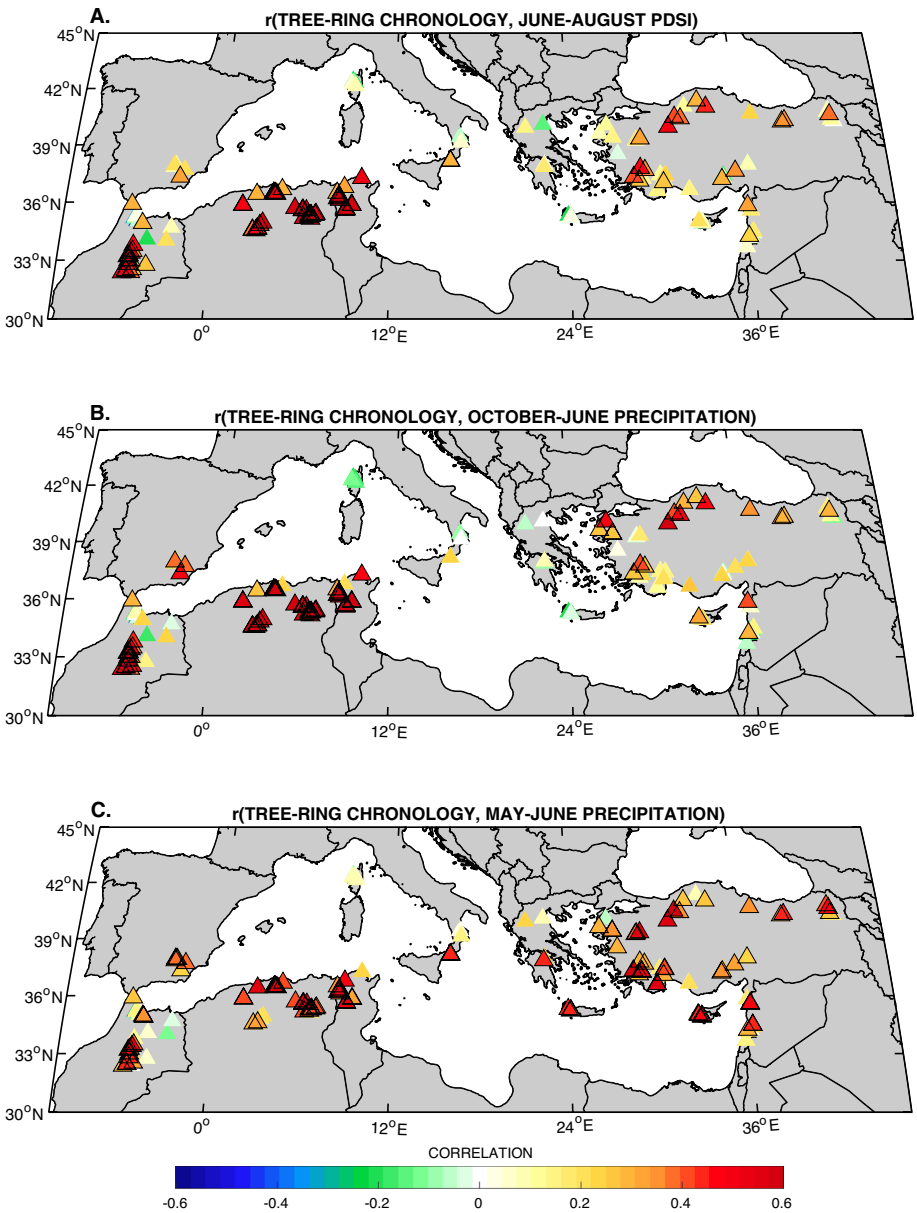

Fig. 2 Site-local correlations between tree-ring chronologies and the (**A**) June through August mean CRU TS4.04 PDSI (van der Schrier et al. 2013; Barichivich et al. 2020), (**B**) October through June total CRU TS4.04 precipitation, and (**C**) total May and June CRU TS4.04 precipitation (Harris et al. 2020). For each tree-ring chronology, the Pearson correlation (color shading) shown in the plot is over the period of overlap between that chronology and the 1940–2019 data from the closest grid point in the data product, and both the chronology and climate data are first-differenced prior to the calculation to isolate the high frequency variability and avoid the influence of trends in either dataset. The calculation is made for the period from 1940 onward to be consistent with the calibration and validation period used in this study, but spatial patterns are similar if the full period is used instead. Tree-ring sites where the correlation with climate is significant at $p < 0.05$ are outlined in black

calibration and validation scores in northwestern Africa extending into southeastern Europe back through 1200 CE (Fig. 5). Indeed, in additional experiments (not shown), we continue to maintain skill in this region back into the first millennium of the Common Era (Touchan et al. 2008a, 2011). Southern Turkey, the Aegean region, and part of the Balkan also maintain reasonably high calibration skill back into the 1200s, but validation skill declines and the earliest part of the reconstruction in this part of the region shows the reconstruction resolving 20% or less of the validation period variance (Fig. 5). The Levant shows similar patterns, with validation R^2 of only 0.15 to 0.20 by the earliest part of the reconstruction. Using the early calibration period (1940 to 1969) and a recent validation period (Fig. 5), largely similar patterns emerge.

As an additional assessment of our ensemble reconstruction, we can evaluate the interseries correlation between the ensemble members for the different search radii. This reveals the influence of the choice of the search radii on the resulting reconstruction. Figure 7 shows the maps of the correlation at each point in the seven ensemble members over their common period of reconstruction. Ensemble members are highly similar ($r > 0.9$) for regions with long and strongly drought sensitive chronologies in Morocco, Algeria, and southern Turkey. In Fig. 7, the areas of high correlation at the very margins of our reconstruction domain simply reflect the limited number of ensemble members with values in that grid point.

In order to assess the broad-scale drought signals present in our reconstruction, we calculated the leading principal

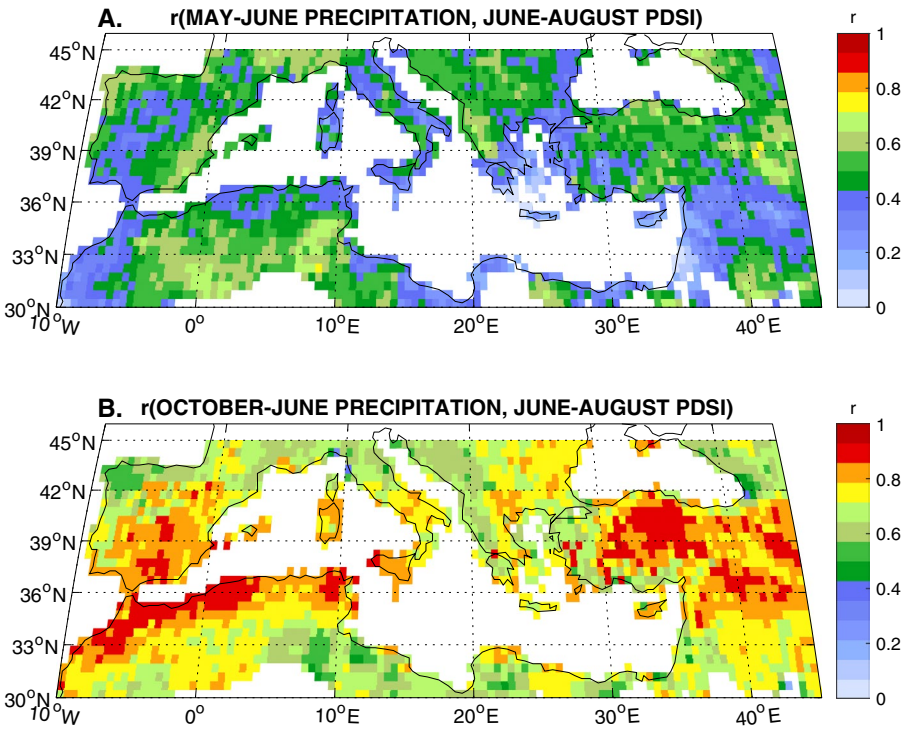

Fig. 3 Pairwise Pearson correlations at each grid point in our study domain between (**A**) total May and June CRU TS4.04 precipitation and CRU summer (JJA) PDSI, and (**B**) total October through June CRU TS4.04 precipitation and CRU summer (JJA) PDSI (Barichivich et al. 2020); Harris et al. 2020). Results shown are for the period from 1940 to 2019 to be consistent with the calibration and validation period used in this study, but spatial patterns are similar if the full period (1901 to 2019) is used instead

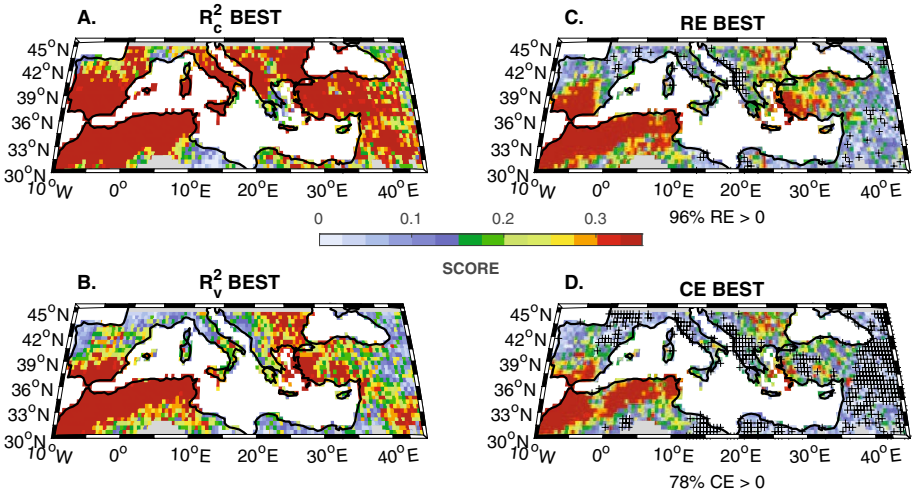

Fig. 4 Reconstruction accuracy and skill scores for the best replicated nest, using 1970 to 2000 for model calibration and 1940 to 1969 for model validation. (**A**) The adjusted R^2 of the calibration, (**B**) is the validation period R^2, **C** is the Reduction of Error (RE), validation period R^2 is the Reduction of Error (RE), and **D** is the Coefficient of Efficiency (CE). Reported below (**C**) and (**D**) is the percent of grid points with scores greater than zero for that metric. Cross-hatching in panels (**C**) and (**D**) shows where the score for that grid point is less than or equal to zero

components (PCs) of both our reconstruction and the target field (Fig. 8). The leading two PCs describe 16% and 15% of the variance in the reconstructed field, respectively, back to 1300 CE (Fig. 8A, B). PC1 of the observed PDSI correlates positively with the observed field over most of the domain (Fig. 8A, C), with particularly strong correlations over northwestern Africa, Spain, Italy, and the Balkans. PC1 of the reconstruction correlates similarly with the observed PDSI field, with the highest values of northwestern Africa (Fig. 8A, E). This PC1 pattern resembles that synchronous basin-wide hydroclimate anomaly patterns identified by both Cook et al. (2016) and Anchukaitis et al. (2019). Anchukaitis et al. (2019) showed that synchronous droughts across the region were associated with a stronger North

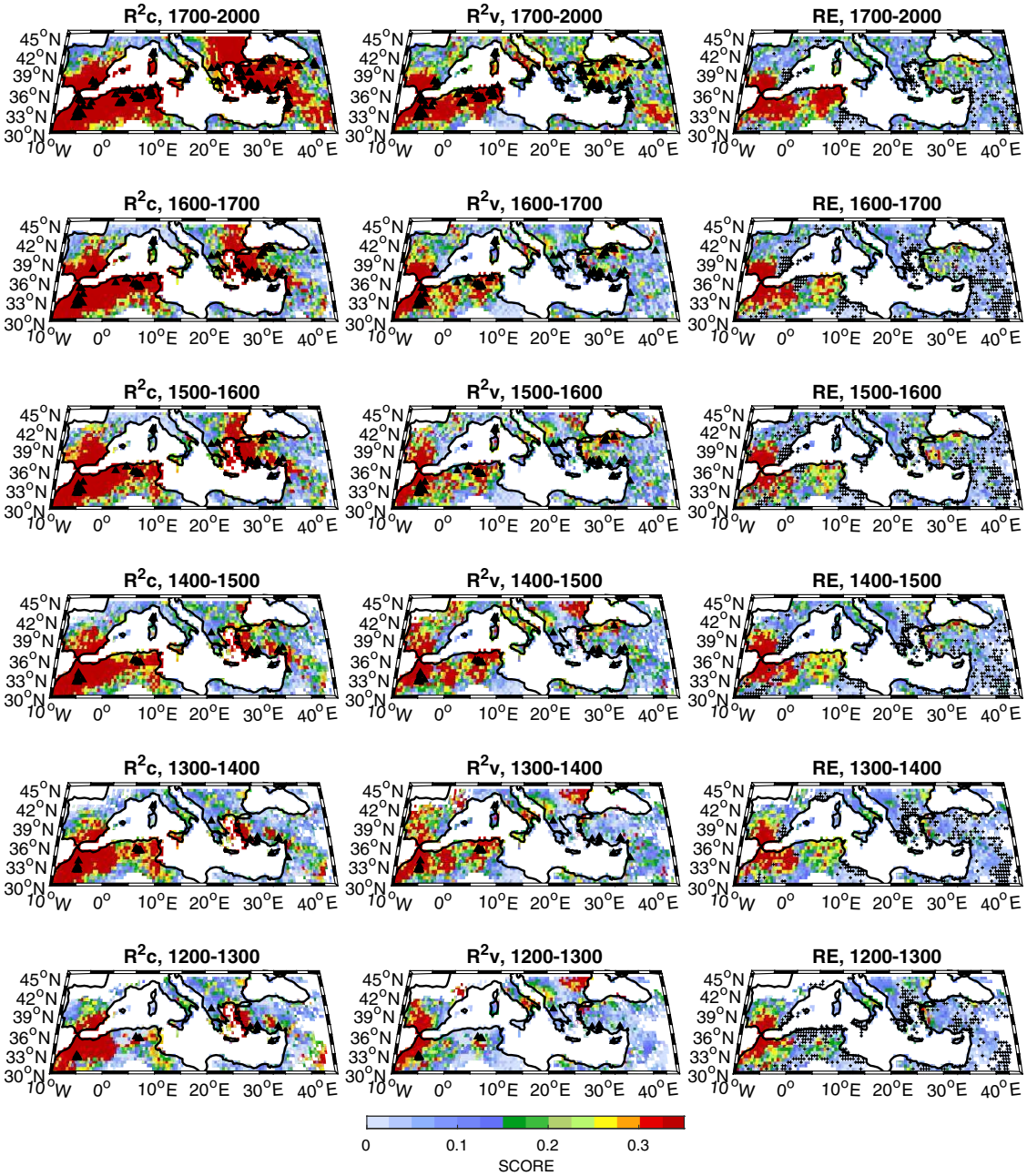

Fig. 5 Time-slice reconstruction accuracy and skill scores, using 1970 to 2000 for model calibration and 1940 to 1969 for model validation (Late Calibration, Early Validation). The left column is the adjusted R^2 of the calibration, the middle column is the validation R^2, and the right column is the Reduction of Error (RE). Rows are the time slices, starting with the period from 1700 to 2000, and going further back in time by a century for each subsequent row. Note that although the last row shown here is the period 1200 to 1300 CE, in northwestern Africa reconstruction skill across all metrics is possible back to at least 1000 CE. Cross-hatching in the last column shows where the RE score for that grid point is less than or equal to zero

Atlantic surface pressure gradient and upper level winds are shifted northward, a pattern similar to that associated with the positive phase of the NAO (see also Dünkeloh and Jacobeit 2003). The time series of the reconstructed and observed PC1 are highly correlated over their period of overlap (Fig. 8A; $r = 0.80$, $p < 0.001$, $N = 71$). PC2 of the observed field shows a dipole with negative correlations over Anatolia and positive correlations over northwestern Africa (Fig. 8D). PC2 of the reconstruction shows weaker correlations overall, although a similar spatial pattern emerges (Fig. 8F). As a result of these differences, however, the second PC of the reconstructed and observed PDSI field are

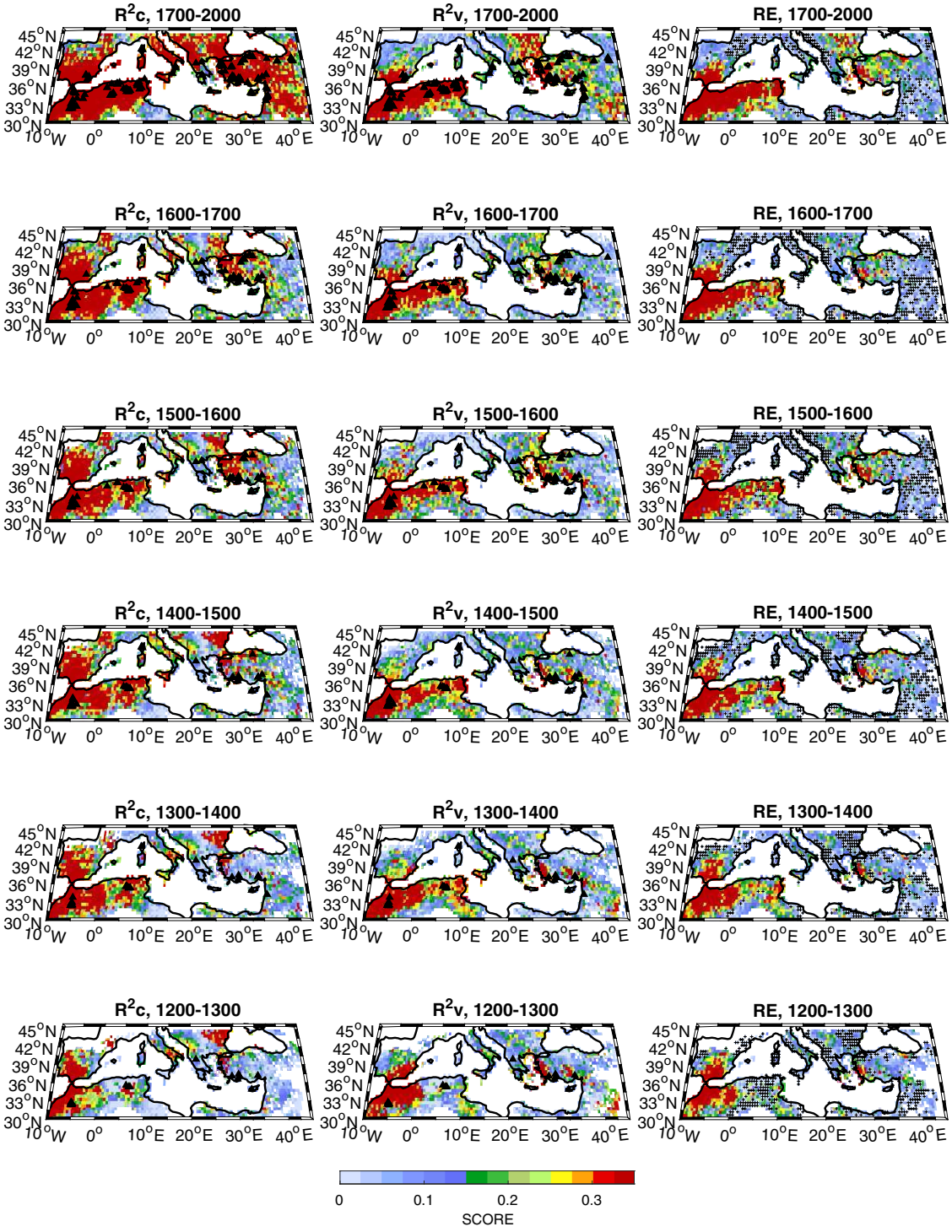

Fig. 6 Time-slice reconstruction accuracy and skill scores, using 1940 to 1969 for model calibration and 1970 to 2000 for model validation (Early Calibration, Late Validation). The left column is the adjusted R^2 of the calibration, the middle column is the validation R^2, and the right column is the Reduction of Error (RE). Rows are the time slices, starting with the period from 1700 to 2000, and going further back in time by a century for each subsequent row. Note that although the last row shown here is the period 1200 to 1300 CE, in northwestern Africa reconstruction skill across all metrics is possible back to at least 1000 CE. Cross-hatching in the last column shows where the RE score for that grid point is less than or equal to zero

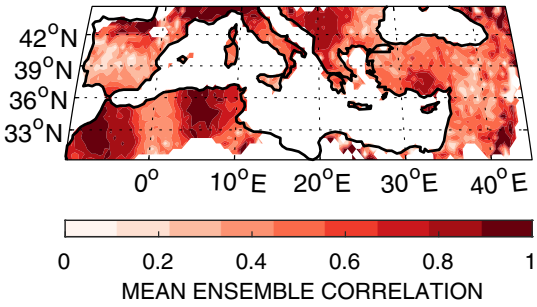

Fig. 7 Mean interseries correlation between search radius ensemble members (400, 500, 600, 700, 800, 900, and 1000 km) for the PDSI reconstruction. The plotted value is the average of the correlation between all ensemble members for the reconstructed PDSI values at each grid. Note that areas of apparently high correlation at the very margins of the reconstruction domain actually reflect the limited number of ensemble members with values in that grid point associated with smaller search radii

less strongly correlated ($r = 0.56$, $p < 0.001$, $N = 71$). A dipole is the expected pattern here in the 2nd mode arising from an unrotated principal components analysis, and may not be simply interpretable as linked to a distinct climatic cause (Monahan et al. 2009); however, Seim et al. (2015) also identified an east–west dipole pattern in Mediterranean pine growth, which they hypothesizes could be influenced by several potential ocean–atmosphere causes. Dorado-Liñán et al. (2017) linked east–west growth differences to the Summer North Atlantic Oscillation (SNAO). Kutiel et al. (1996) and Xoplaki et al. (2004) also identified east–west dipole patterns in instrumental data that they linked to atmospheric circulation.

Our reconstruction is most accurate and shows the most consistent skill in the western Mediterranean region over most of the last millennium (Figs. 4, 5, 6, 8). Comparison of the time series from the reconstruction with the corresponding instrumental data from the western Mediterranean (32–42N, 10W to 0E, following Cook et al. 2016) as well as an extended western Mediterranean region encompassing Algeria and Tunisia (32-42N, 10W to 10E) show strong correlations between the target PDSI data and the reconstruction over the entire region (Fig. 9, $r = 0.82$ and $r = 0.74$, respectively, $N = 71$, $p < 0.001$).

3.3 Comparisons to the old world drought atlas

Pointwise correlations between our reconstructed PDSI field and the OWDA reveal regions of both similarity and differences (Figs. 10, 11), with these patterns observed despite the changing search radii across our ensemble. Areas of the greatest similarly are Morocco, southern Spain, the Balkans, and Anatolia. These are also the regions most similar to one another across our ensemble members themselves. Substantially lower correlations are observed distal from the longest and most drought sensitive chronologies in regions of the Levant, coastal Libya and Egypt, and northern Spain. As might be expected (c.f. Knutti et al. 2010; Christiansen 2019), our ensemble mean reconstruction shows the best correlation overall with the OWDA, with regions of highest agreement over Morocco and southern Spain, the Balkans, and much of Anatolia (Fig. 10). Considering just the dominant patterns of our reconstruction, our leading mode of variability (PC1) captures similar variability as the OWDA in the western Mediterranean, Greece, and Turkey, while PC2 is similar to the OWDA only over Anatolia (Fig. 11) and does not reproduce the dipole patterns shown in Fig. 8D and 8F.

One region of notable disagreement between our reconstruction and the OWDA is the Levant, which is important because this region has been previously identified as having a drying trend that took its drought severity outside the range of variability for the last millennium (Cook et al. 2016). Fig. 12 shows the comparison between the reconstructed OWDA time series for the region (Fig. 12A, C) and our reconstruction (Fig. 12B, C). When the regional average of the reconstructed PDSI fields are correlated against the corresponding reconstructed fields themselves (Fig. 12A, B), both reveal regions of high correlation over the Levant, although the OWDA's region of correlation extends westward through Libya and has an opposite sign dipole correlation over the Balkans. The high correlations for our ensemble mean reconstruction are confined largely to the Levant itself and parts of Turkey, with low and non-significant correlation throughout the more distal parts of our domain. Interestingly, the Levant time series from our reconstruction and from the OWDA are significantly and highly correlated with the observations during the instrumental period ($r = 0.64$ and $r = 0.63$, respectively, $N = 71$, $p < 0.001$), but show greater disagreement prior to that time ($r = 0.28$, $p < 0.001$).

3.4 Recent droughts in a long-term context

We repeated the analysis of recent drought severity compared to the tree-ring reconstructed series from Cook et al. (2016). In Cook et al. (2016), the timing and duration of these events was determined from a 10-year loess smooth applied to the PDSI data through the end of the OWDA record in 2012, which allows for intervening individual wet years but emphasizes decadal-scale periods of negative mean values. For the Levant, we identified three recent drought periods – the original period used by Cook et al. (2016) from 1998 to 2012, the most recent epoch of strong drought from 2004 to 2018, and then the continuous period spanning 1998 to 2018. For the western Mediterranean (Fig. 9) we use the

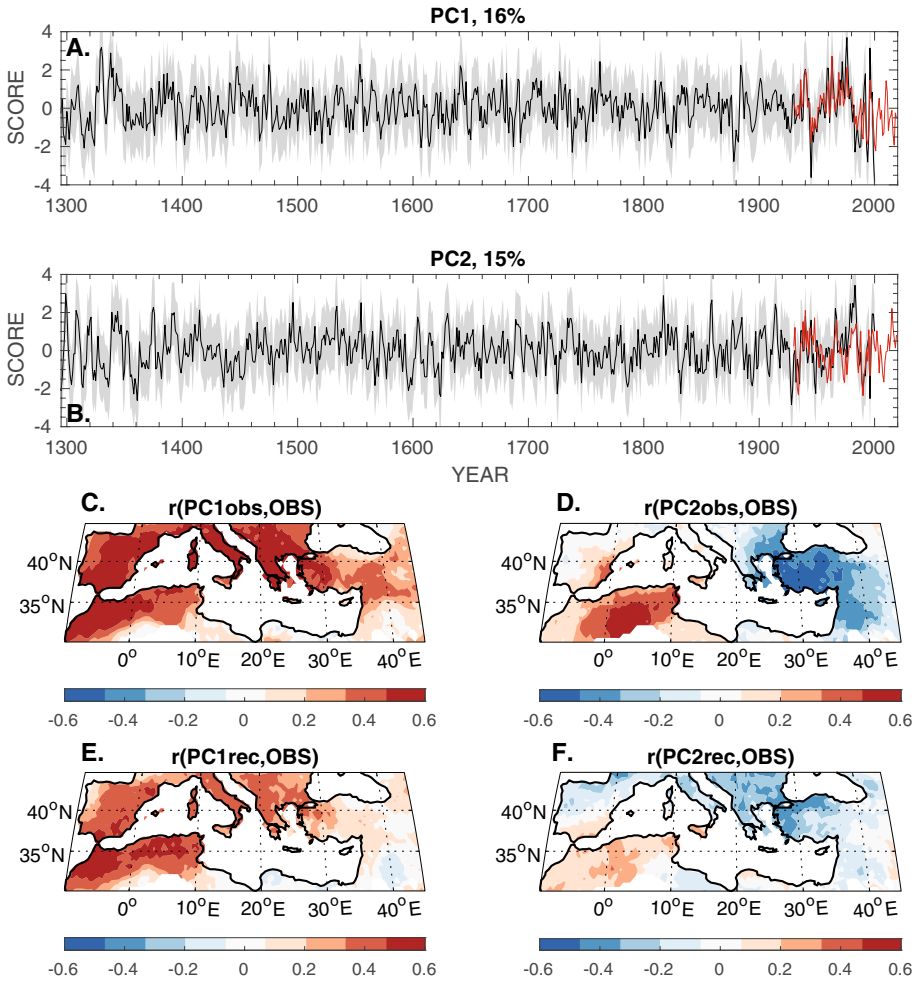

Fig. 8 Leading modes of reconstructed drought variability from observations and our tree-ring reconstruction. (**A**) The time series expansion of the leading mode (PC1) from the reconstruction (black) and gridded observational data (red). (**B**) The time series expansion of the second mode (PC2) of spatiotemporal variability from the reconstruction (black) and gridded observational data (red). The uncertainties (gray shading) in panels (**A**) and (**B**) are estimated as 2 times the field correlation-weighted (weights are from panels **E** and **F**) root mean squared error of validation at each reconstructed grid point through time. Panels (**C**) and (**D**) show the correlation between PC1 and PC2 respectively from the observation data with the observational field (effectively, a ways of visualizing the spatial loading of these modes). Panels (**E**) and (**F**) show the correlation between PC1 and PC2 respectively from our tree-ring reconstruction with the observational field (effectively, a ways of visualizing how well the reconstruction represents larger patterns of the observed PDSI variability)

original drought from Cook et al. (2016) from 1980 to 2009, as well as the continuation of this dry period through 2018.

In all five cases considered, these most recent droughts are more severe on average than any prior period of severe drought identified from the most reliable period of our tree-ring reconstruction since 1300 (Fig. 13). However, in none of these cases is the most recent drought significantly different based on the simple t-test ($p > 0.05$). Based on our non-parametric resampling procedure, in the western Mediterranean the most recent late 20th and early 21st century droughts from 1980 to 2009 and 1980 to 2018 are the most severe in 88% and 83% of the bootstrapped means, respectively, compared to prior droughts of the same duration. For the Levant, the 1998 to 2012 period is the most severe in 70% of the paired bootstrapped samples, while the 2004 to 2018 and the extended 1998 to 2018 droughts are the most severe in 82% and 88%, respectively. Thus, while recent droughts in both the western Mediterranean and Levant have mean PDSI values that make them the most severe since at least 1300 CE, uncertainty in our reconstruction keeps these droughts from exceeding conventional significance levels.

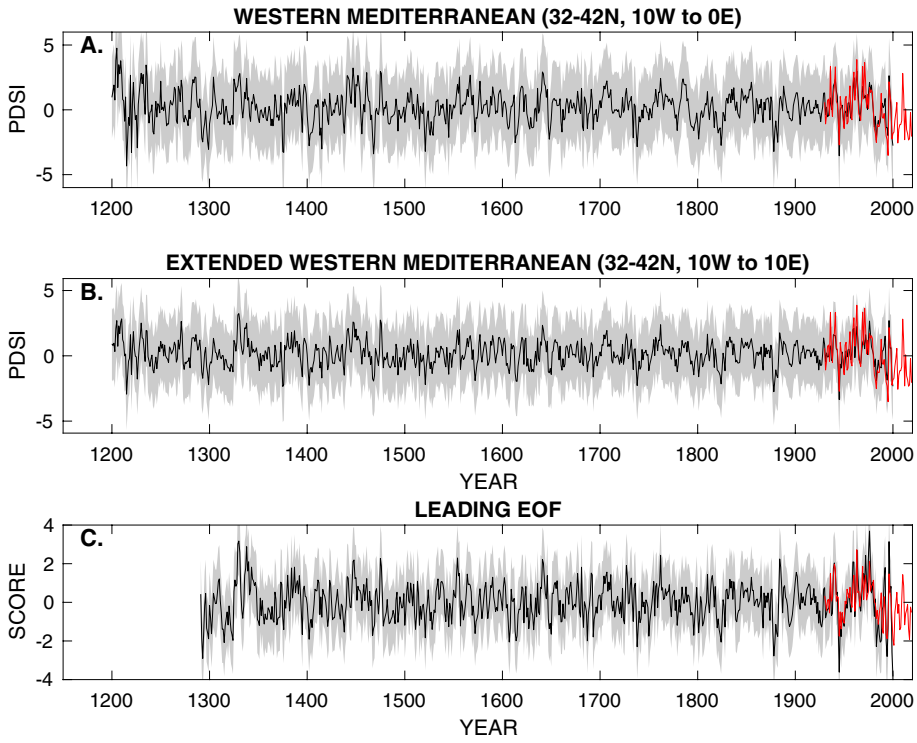

Fig. 9 Time series of reconstructed and observed drought in the western Mediterranean. Reconstructed (black line) and observed (red line) for mean JJA PDSI over the (**A**) western Mediterranean region used in Cook et al. (2016) and (**B**) an extended western Mediterranean region also encompassing Algeria and Tunisia to the east. The uncertainties (gray shading) in panels (**A**) and (**B**) are estimated as 2 times regional mean root mean squared error of validation. **C** As in Fig. 9A, the leading (PC1) time series of the reconstructed and observed fields are also well-correlated during their period of overlap and reflect drought variability primarily but not exclusively, over northwestern Africa and southern Spain (see also Fig. 8E)

4 Discussion

4.1 Strengths and weakness of the tree-ring network

Our tree-ring chronologies (Fig. 1) reflect a broad network from more than a dozen species and 10 countries across the Mediterranean. This mix of species, elevations, and site characteristics comprise a range of hydroclimate responses (c.f. Griggs et al. 2007; Büntgen et al. 2010; Touchan et al. 2012; Köse et al. 2012; Galván et al. 2014; Touchan et al. 2014a; DeSoto et al. 2014; Touchan et al. 2016; Pacheco et al. 2016; Martin-Benito et al. 2016, 2017; Touchan et al. 2017; Martin-Benito et al. 2018), although common features emerge (Fig. 2). In the western Mediterranean, the most climate sensitive tree-ring chronologies tend to be *Pinus halepensis* and *Cedrus atlantica* in the High Atlas, Saharan Atlas, and Aurès Mountains of Morocco, Algeria, and Tunisia (Touchan et al. 2017). Long chronologies sensitive to winter and water-year precipitation (Fig. 2B) from *C. atlantica* in particular allow the sustained skillful PDSI reconstructions back to at least 1200 CE seen in Figs. 4, 5, and 6. Coastal and lower elevation chronologies in north Africa have a more muted drought signal in this region, but in southeastern Spain our limited collection of *Pinus halepensis* and *Pinus nigra* show significant water-year correlations (Touchan et al. 2017) that allow them to contribute significant information to western Mediterranean reconstruction accuracy and skill over the most recent reconstruction nests (Fig. 2A, B). Our Corsican *Pinus nigra* chronologies appear to have a very weak climate signal (Fig. 2); however, Esper et al. (2022) have recently developed a hydroclimate-sensitive millennium length chronology from treeline *Pinus nigra* in Corsica and found a previous year growing season PDSI signal, but also noted the challenge in identifying a robust precipitation signal in their chronology due to limited meteorological data.

In the eastern Mediterranean, the narrow window of May through July precipitation sensitivity in much of the tree-ring network (Touchan et al. 2003; Akkemik et al. 2008; Köse et al. 2011; Touchan et al. 2014a, c; Martin-Benito et al. 2016) leads to an overall weaker association with PDSI compared with spring-summer rainfall alone (Fig. 2A, C, 5, 6). While these months are important for agriculture in the region, this sensitivity leads to lower calibration and validation values in the region when targeting JJA PDSI for the reconstruction over the entire domain (Fig. 3). The Levant also has relatively few tree-ring chronologies, despite the importance of climate change and variability here for agriculture, migration, and potentially conflict (for differing views on the latter, see for instance Gleick 2014; Kelley et al. 2015; Selby et al. 2017; Ide 2018). In addition to sites in Cyprus (Griggs et al. 2007; Touchan et al. 2014b; Coulthard et al. 2017), several tree-ring chronologies are available from Lebanon, Jordan, and Syria (Touchan and Hughes 1999; Touchan et al. 1999b, 2005b, 2014c) and were used in the OWDA; however, most of these chronologies have not been recently updated

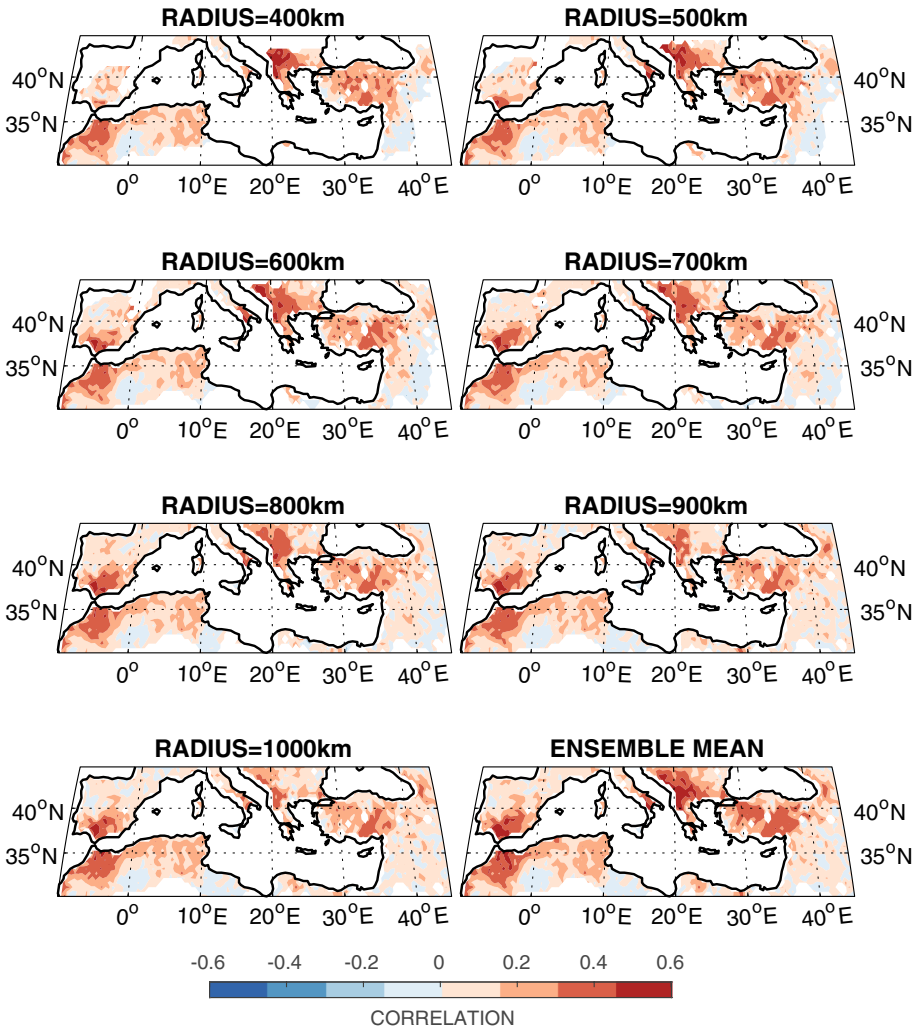

Fig. 10 Pointwise field correlation between our reconstruction and the OWDA. Each panel corresponds to a reconstruction ensemble member with a different search radius for PPR and the bottom right panel shows the spatial correlation between the OWDA and our reconstruction ensemble mean field

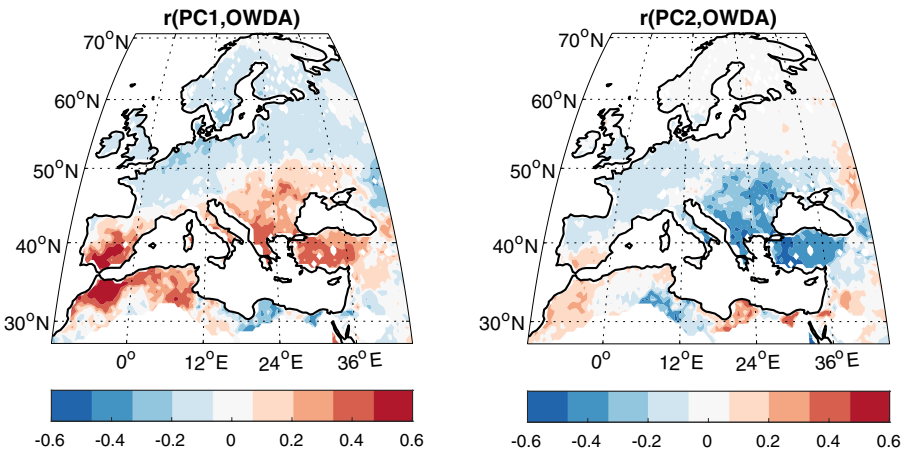

Fig. 11 Spatial correlations between the 1st (left panel) and 2nd (right panel) PC of our reconstruction and the OWDA drought field over the period 1300 to 2000

and do not extend even to 2000, limiting their use for calibration against the most recent meteorological records. Updating and possibly extending tree-ring chronologies in the Levant should be a priority when conditions allow.

4.2 Comparisons to the old world drought atlas

Our reconstruction shows regions of substantial agreement with the OWDA but also areas where the two fields are

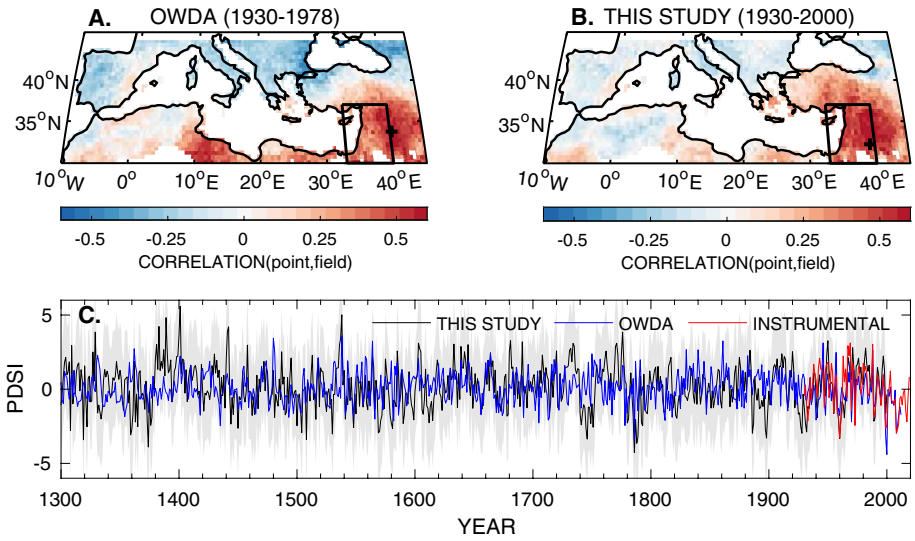

Fig. 12 Levant drought reconstruction in this study and the OWDA. **A** Correlation of the mean time series of Levant drought (averaged over the black box, 30–37N, 33 to 40E from Cook et al. (2016)) against the instrumental JJA PDSI field from Barichivich et al. (2020). **B** As in panel (**A**), except the average Levant time series of our ensemble mean PDSI reconstruction is correlated against the observed JJA PDSI field. In both panels the time span over which the field correlation is calculated is limited to the period since 1930 (when instrumental data are more reliable) and the last year where the reconstruction is reconstructed entirely from tree ring data (indicated by the date range above each panel). The black crosses indicate the grid point with the highest correlation between the box average JJA PDSI value and the observed PDSI field for each reconstruction. **C** Time series of the box averaged Levant PDSI values for our reconstruction (black line), the OWDA (blue line), and the gridded observational data (red line). The uncertainties on our reconstruction (gray shading) in panels (**C**) are estimated as 2 times regional mean root mean squared error of validation

only weakly similar (Fig. 10). Perhaps not surprisingly, the strongest correlations and highest similaritities are in regions with long and strongly PDSI-sensitive tree-ring chronologies, particularly within the search radii for grid points in the High Atlas of Morocco and parts of Turkey and the Balkans. In these regions, long climate-sensitive chronologies common to both datasets dominate the reconstructed signal through time (Figs. 1 and 2). One region of interest is Algeria and Tunisia where our tree-ring network has long drought sensitive chronologies but the correlation with the OWDA is relatively low. The OWDA does have two chronologies in Algeria (Cook et al. 2015), one of them stretching back into the first millennium of the Common Era that is also part of our network (Theniet Zamroune). However, our network also has substantially more chronologies in the Saharan Atlas mountains as well as chronologies from Tunisia that are not included in the OWDA, which is likely responsible for the relatively low correlation values there. Future versions of the OWDA or other hemisphere-scale PDSI reconstructions can benefit from the inclusion of our new chronologies from this region.

The largest discrepancies between the OWDA and our reconstruction come either from the periphery of our network (where the OWDA can draw on a set of nearby European chronologies that fall outside of our domain) and the eastern Mediterranean and the Levant in particular. The eastern Mediterranean is in general a region of lower accuracy and skill in both our reconstruction and in the OWDA (Figs. 4, 56; and see also Fig. S11 in Cook et al. (2015)). Indeed, our reconstruction has somewhat higher skill as measured by RE and CE over the most recent centuries in the eastern Mediterranean outside of Turkey, although both products have low validation scores in the Levant and a relatively limited number of local chronologies available. It is likely also that differences in how the PPR method is applied play a role in the low correlation between the two drought reconstructions. Our procedure limits the largest search radius in the ensemble to 1000 km, whereas to be able to use a minimum of 20 chronologies the OWDA has to use a larger search radius (1500 km or greater) for grid points at the periphery of the reconstructed domain in northeastern Africa and the Levant. This likely explains the differing spatial correlation patterns seen both for PC2 in Fig. 8 and in Fig. 12. Our Levant time series shows a decline in spatial correlation between reconstruction and the target PDSI field moving away from the region, with low and insignificant values in western Turkey and north Africa. The OWDA, in contrast, shows significant positive correlations all the way to Libya and a change in sign in the Balkans to a significant negative correlation. One possible explanation for these differing patterns is the influence of the search radii (and the minimum chronology requirement), which in the OWDA can draw on chronologies further away in central Europe and on which grid points in Libya and Egypt similarly rely. In

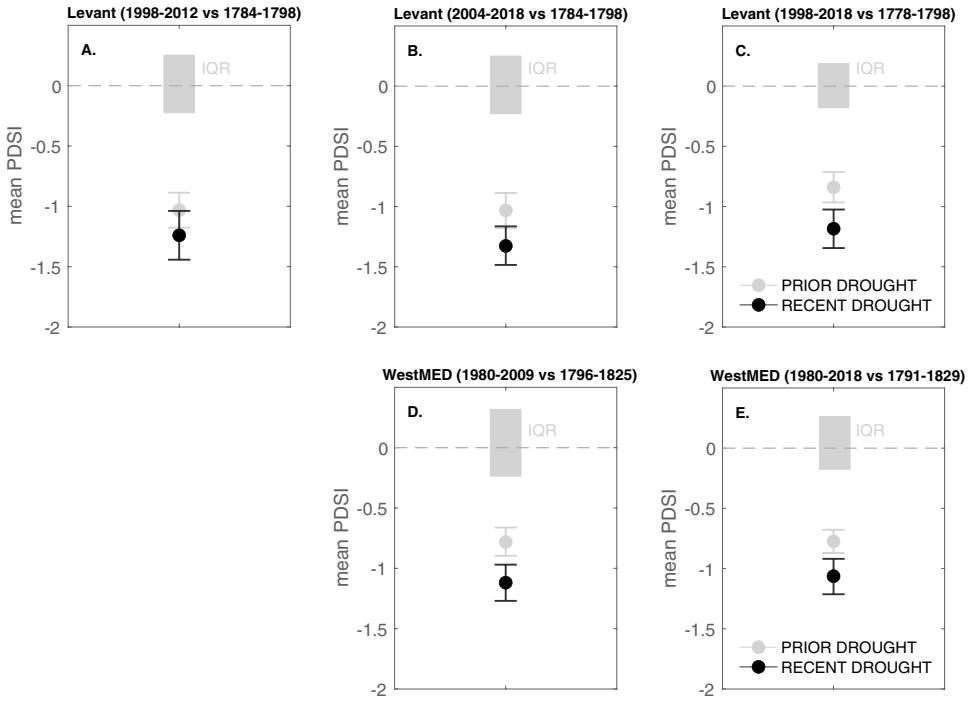

Fig. 13 Following Cook et al. (2016), comparisons of multiyear average recentered PDSI during recent decadal-scale drought periods identified in the observational period (black dots) and the driest previous periods of the same length from 1300 to 2012 C.E. in our reconstruction (gray dots). Shaded gray bars are the interquartile range (IQR) of mean PDSI values for all moving windows of the same length in each region. Whiskers are the 25th and 75th confidence limits for the selected dry events, calculated using bootstrapping of the estimated mean value with 10,000 draws with replacement from PDSI values during these intervals. Panels A through C show this analysis applied to recent drought period we identify in the Levant (30–37N, 33 to 40E), and panels D end E show this analysis applied to drought periods identified in the western Mediterranean (32–42N, 10W to 0E). Differences in the absolute value of the drought severity between our reconstruction and those shown in Cook et al. (2016) are due to the effect of re-normalizing the time series over the length of the reconstruction used in this analysis, which differs from the length of the reconstruction available in the OWDA

particular the dipole structure of the OWDA's Levant spatial correlation suggests that the reconstruction in that region leverages negative covariance between the eastern Mediterranean and European drought (e.g. Anchukaitis et al. 2019; Baek et al. 2020).

The difference between our Levant reconstruction and that of the OWDA influences the analysis of recent drought severity (Fig. 13). For all three time periods considered, the recent drought still has a mean value in our reconstruction that makes it the most severe on record, similar to the findings of Cook et al. (2016). However, in the case of our reconstruction, both parametric and non-parametric significance tests fail to rule out at conventional confidence levels that a previous Levant drought of similar length could have been as or more severe, within uncertainty. The preponderance of the evidence, particularly the non-parametric bootstrap test of the mean, still suggests that the modern drought is likely to be the most severe in at least seven centuries, but differences in the reconstruction over time are sufficient to increase uncertainty enough to affect the significance tests. Similarly, for the two periods considered in the western Mediterranean, the mean PDSI values also suggest the recent droughts are again the most severe on record, but the uncertainty is large enough that again both significance tests fail to rule out a prior drought with similar severity. That the long reconstructed PDSI time series in both regions show recent drying trends and drought events (Fig. 9 and 12) that are consistent with expectations from anthropogenic warming yet not able to be completely separated from the potential influence of natural variability (Kelley et al. 2012b, 2015; Cook et al. 2020a) emphasizes the importance of paleoclimate reconstructions for better characterizing the range of internal variability in the system.

4.3 Sources of uncertainty and future directions

There are a number of sources of uncertainty that can contribute to the difference here between the OWDA and our reconstruction. First, the composition of the proxy network is a major source of uncertainty (Fig. 1). The OWDA uses fewer but on average longer tree-ring chronologies and requires a minimum number of starting chronologies in the

most recent nest, but as a consequence some distal regions of the domain may draw on chronologies more than 1000 km away from that grid point. This reflects a real and weakly constrained trade-off in terms of low frequency preservation, predictor sample size and sample stability, assumptions about the stability of the large-scale covariance, and capture of local vs. regional climate signals. Future iterations of the OWDA or similar drought atlases may wish to draw on some or all of the chronologies currently in our network that are not yet part of their collection. Similarly, new or existing chronologies from other research groups (e.g. Tejedor et al. 2016, 2017; Leonelli et al. 2017; Klippel et al. 2017, 2018; Martin-Benito et al. 2018; Esper et al. 2022) can enhance the proxy network in the future and perhaps expand the spatial skill. When possible, updates to Levant chronologies in particular (e.g. Touchan and Hughes 1999) would also provide critical new proxy information.

Choices made during the statistical reconstruction procedure can also have an important influence, even when applied to a similar network of tree-ring proxies (Büntgen et al. 2021; Anchukaitis and Smerdon 2022). While the PPR methods used here and in the OWDA (Cook et al. 2015) are fundamentally similar, there are choices to be made during its use, including calibration and validation periods, the level of pre-screening of predictors, and model selection rules, amongst others. Smerdon et al. (2015) showed that in places where the tree-ring network comprises long highly climate-sensitive tree-ring chronologies, the interpretations of past and present drought are robust to a range of methodological choices. However, in the situation where the proxy data are relatively sparse or the climate target of interest varies from the primary seasonal sensitivity of the proxies (Fig. 2), the methodology can influence the reconstruction more strongly. That our reconstruction is most robust across ensemble members (Fig. 7) and most similar to the OWDA in the locations where there are long and strongly PDSI-sensitive chronologies (Fig. 10) suggests that the composition of the proxy network is the primary cause of the difference, although this is almost certainly mediated by methodological choices such as the search radius, sample depth requirements, and chronology weighting used in the OWDA. The OWDA also applies signal free (SF) detrending to the tree-ring measurements to develop the chronologies (Melvin and Briffa 2008), including both individual and regional curve detrending (Cook et al. 2015). While this might in theory explain some differences between the reconstruction, McPartland et al. (2020) found insignificant differences in a moisture-sensitive network of tree-ring data from North America when signal free and conventional methods were applied. Furthermore, comparison of the Levant reconstruction time series between the reconstructions (Fig. 12) suggests that the OWDA actually has less medium-term variability. In the future, methodological comparisons, pseudoproxy studies, and sensitivity testing (e.g. Smerdon et al. 2015; Steiger et al. 2018; King et al. 2021) conducted at the same time as future reconstructions could help clarify the relative role of proxy network and methodological choices in causing differences between reconstruction of similar fields.

Although not explicitly discussed above, we are also aware of differences in the available gridded target datasets. Here we use the high resolution self-calibrated gridded PDSI from van der Schrier et al. (2013) as updated by Barichivich et al. (2020). In preparation for our reconstruction, we also compared an upscaled (2.5^o) version of our target dataset with the PDSI data developed by Dai (2011). We found a broad range of pointwise correlations across the Mediterranean between the two datasets for the period 1901 to 2011, including values at some grid points in the Levant and marginal areas of the Sahara as low as $r < 0.25$ (not shown). This suggests that the calculation of gridded PDSI can be sensitive to the choice or resolution of input datasets and/or parameters (van der Schrier et al. 2013; Trenberth et al. 2014; Vicente-Serrano et al. 2015; Dai and Zhao 2017), particularly in times and places where original station data are sparse or uncertain (Zhang et al. 2005; Kuglitsch et al. 2009; Tanarhte et al. 2012; Beguería et al. 2016). Uncertainty in the calculation and choice of the target dataset play an additional role in influencing both calibration and validation accuracy and skill as well.

5 Summary and conclusions

We reconstruct summer PDSI for the Mediterranean Basin over much of the last millennium using a large network of tree-ring chronologies from the region. The reconstruction shows especially high skill over the full period in the western Mediterranean, including strong coherence between the leading spatiotemporal mode of PDSI variability in observations, the OWDA, and our reconstruction. Northwestern Africa in particular has robust reconstruction metrics back through much of the last millennium. The skill in reconstructing summer PDSI in the eastern Mediterranean, including the Levant, is more limited in part due to the narrower window of seasonal precipitation response in the tree-ring chronologies in that part of the region. Our new reconstruction supports earlier studies in suggesting that the recent drought in both northwestern Africa and the Levant is unprecedented in severity in the tree-ring record. However, difference between the OWDA and our reconstruction, particularly in the Levant modify our conclusions about whether recent severe droughts are statistically significantly more severe than that period of similar length drought earlier in the reconstruction. Uncertainty in the reconstructions as well as the presence of

internal hydroclimate variability at decadal time scales influences the strength of the inference about the exceptional nature of the most recent dry periods.

Our reconstruction highlights both the value of additional chronologies for reconstructing Mediterranean hydroclimate in time and space and the sensitivity of analyses of internal PDSI variability to the underlying network and methodological choices of the reconstruction. Future dendroclimatology research in the region might also benefit from further use of sub-annual or wood anatomical data to resolve seasonal signals across the domain (e.g. Meko and Baisan 2001; Piermattei et al. 2020). Our tree-ring network here and the insights our reconstruction provides allow for an updated and more extensive set of proxy data to be used for future large-scale drought reconstructions across the Mediterranean, Europe, and the entire Northern Hemisphere.

Acknowledgements The authors wish to thank in Morocco (Ministry of Agriculture and the National School of Forest Engineering), Algeria (General Directorate of Forestry, Conservators of the Forests of Batna, National Parks of Belezma, Thniet el Had, Djurdjura, and Chréa), Tunisia (Institute of Sylvo-Pastoral of Tabarka and Institut national de recherche en génie rural, eaux et forêts (l'INRGREF)), Turkey (Ministry of Forestry, Southwest Anatolia Forest Research Institute (SAFRI)), Greece (Forest Protection, School of Forestry and Natural Environment, Aristotle University of Thessaloniki), Cyprus (Ministry of Agriculture, Department of Forestry, Cyprus Forestry College, and Cyprus Meteorological Service), Lebanon (Ministry of Agriculture, Department of Forestry and University of Balamand), Syria (University of Aleppo-Faculty of Agriculture), Southern Italy (Sila National Park and Aspromonte National Park), and Southeastern Spain (Ministry of the Environment and Spatial Planning and Regional Government of Andalusia). We thank Martin Munro for his advice and suggestions. We thank Alexis H. Arizpe, Christopher Baisan, Russell Biggs, Gurudas C. Bock, Jeffrey Balmat, and William E. Wright for their valuable assistance in the field. We thank Jim Burns and William E. Wright for their help in dating part of the tree-ring sites. We also thank Russell Biggs, Victoria L. Frazier, Alicia Stout, Gurudas C. Bock, Jessica L. Little, Anthony P. Trujillo, Jeremy Goral, and Julie Wong for their assistance in sample preparation and measurement.

Author Contributions Kevin Anchukaitis and Ramzi Touchan designed the study. All authors contributed to material preparation and data collection. Analyses were performed by Kevin Anchukaitis, Ramzi Touchan, David Meko, Jordan Krcmaric, and Benjamin Cook. All authors contributed to the writing of the manuscript. All authors read and approved the final manuscript.

Funding Funding to develop the Mediterranean tree-ring network and climate reconstructions was provided by grants from the US National Science Foundation's Earth System History (ESH) and Paleo Perspectives on Climate Change (P2C2) programs, AGS-075956, AGS-0758486, AGS-0317288, AGS-1103314, AGS-1103450, AGS-1501856.

Data Availability Statement All the raw measurements, site chronologies, and reconstructions associated with this manuscript will be archived with NOAA's National Centers for Environmental Information (NCEI) World Data System for Paleoclimatology at https://www.ncei.noaa.gov/products/paleoclimatology upon publication of this manuscript.

Declarations

Conflict of interest The authors have no relevant financial or non-financial interests to disclose.

References

Akkemik Ü, D'Arrigo R, Cherubini P, Köse N, Jacoby GC (2008) Tree-ring reconstructions of precipitation and streamflow for northwestern Turkey. Int J Climatol 28(2):173–183

Allen MR, Ingram WJ (2002) Constraints on future changes in climate and the hydrologic cycle. Nature 419(6903):228–232

Altava-Ortiz V, Llasat MC, Ferrari E, Atencia A, Sirangelo B (2011) Monthly rainfall changes in Central and Western Mediterranean basins, at the end of the 20th and beginning of the 21st centuries. Int J Climatol 31(13):1943–1958

Anchukaitis KJ, Smerdon JE (2022) Progress and uncertainties in global and hemispheric temperature reconstructions of the Common Era. Quat Sci Rev 286(107):537

Anchukaitis KJ, Wilson R, Briffa KR, Buntgen U, Cook ER, D'Arrigo R, Davi N, Esper J, Frank D, Gunnarson BE, Hegerl G, Helama S, Klesse S, Krusic PJ, Linderholm HW, Myglan V, Osborn TJ, Zhang P, Rydval M, Schneider L, Schurer A, Wiles G, Zorita E (2017) Last millennium Northern Hemisphere summer temperatures from tree rings: Part II, spatially resolved reconstructions. Quat Sci Rev 163:1–22. https://doi.org/10.1016/j.quascirev.2017.02.020

Anchukaitis KJ, Cook ER, Cook BI, Pearl J, D'Arrigo R, Wilson R (2019) Coupled Modes of North Atlantic Ocean-Atmosphere Variability and the Onset of the Little Ice Age. Geophys Res Lett 46(21):12,417-12,426

Baek SH, Smerdon JE, Dobrin GC, Naimark JG, Cook ER, Cook BI, Seager R, Cane MA, Scholz SR (2020) A quantitative hydroclimatic context for the European Great Famine of 1315–1317. Nature Commun Earth Environ 1(1):1–7

Barichivich J, Osborn T, Harris I, Schrier Gerard, Jones P (2020) Monitoring global drought using the self-calibrating Palmer Drought Severity Index [in "State of the Climate in 2019''. Bull Am Meteorol Soc 101:51–52

Barkhordarian A, von Storch H, Bhend J (2013) The expectation of future precipitation change over the Mediterranean region is different from what we observe. Climate Dynam 40(1):225–244

Beguería S, Vicente-Serrano SM, Tomás-Burguera M, Maneta M (2016) Bias in the variance of gridded data sets leads to misleading conclusions about changes in climate variability. Int J Climatol 36(9):3413–3422

Büntgen U, Frank D, Trouet V, Esper J (2010) Diverse climate sensitivity of Mediterranean tree-ring width and density. Trees 24(2):261–273

Büntgen U, Allen K, Anchukaitis KJ, Arseneault D, Boucher E, Bräuning A, Chatterjee S, Cherubini P, Corona C, Gennaretti F et al (2021) The influence of decision-making in tree ring-based climate reconstructions. Nature Commun 12(1):1–10

Chenoweth J, Hadjinicolaou P, Bruggeman A, Lelieveld J, Levin Z, Lange MA, Xoplaki E, Hadjikakou M (2011) Impact of climate change on the water resources of the eastern Mediterranean and Middle East region: Modeled 21st century changes and implications. Water Resources Research 47(6)

Christensen J, Hewitson B, Busuioc A, Chen A, Gao X, Held I, Jones P, R K, Kwon W, Laprise R, Magana V, Mearns L, Menendez C, Raisanen J, Rinke A, Sarr A, Whetton P (2007) Regional climate projections. In: Solomon S, Qin D, Manning M, Chen Z, Marquis M, Averyt K, Tignor M, Miller H (eds) Climate Change 2007: The Physical Science Basis. Contribution of

Working Group I to the Fourth Assessment Report of the Intergovernmental Panel on Climate Change, Cambridge University Press, Cambridge, pp 849–926
Christiansen B (2019) Analysis of ensemble mean forecasts: The blessings of high dimensionality. Monthly Weather Review 147(5):1699–1712
Cook BI, Mankin JS, Marvel K, Williams AP, Smerdon JE, Anchukaitis KJ (2020a) Twenty-first century drought projections in the CMIP6 forcing scenarios. Earth's Future 8(6):e2019EF001,461
Cook BI, Smerdon JE, Cook ER, Williams AP, Anchukaitis KJ, Mankin JS, Allen K, Andreu-Hayles L, Ault TR, Belmecheri S et al (2022) Megadroughts in the common Era and the anthropocene. Nature Rev Earth Environ, 1–17
Cook ER (1985) A Time Series Approach to Tree-Ring Standardization. PhD thesis, University of Arizona, Tucson, AZ, USA
Cook ER, Briffa KR (1990) A comparison of some tree-ring standardization methods. In: Kairiukstis LA (ed) Methods of Dendrochronology. Kluwer, Dordrecht, pp 104–123
Cook E, Kairiūkštis L (eds) (1990) Methods of dendrochronology: applications in the environmental sciences. Kluwer Academic, Doredrecht
Cook ER, Meko DM, Stahle DW, Cleaveland MK (1999) Drought reconstructions for the continental United States. J Clim 12(4):1145–1162
Cook ER, Woodhouse CA, Eakin CM, Meko DM, Stahle D (2004) Long-term aridity changes in the western United States. Science 306(5698):1015–1018
Cook ER, Anchukaitis KJ, Buckley BM, D'Arrigo RD, Jacoby GC, Wright WE (2010) Asian Monsoon Failure and Megadrought During the Last Millennium. Science 328(5977):486–489. https://doi.org/10.1126/science.1185188
Cook ER, Seager R, Heim RR Jr, Vose RS, Herweijer C, Woodhouse C (2010) Megadroughts in North America: Placing IPCC projections of hydroclimatic change in a long-term palaeoclimate context. J Quat Sci 25(1):48–61
Cook BI, Cook ER, Anchukaitis KJ, Seager R, Miller RL (2011) Forced and unforced variability of twentieth century North American droughts and pluvials. Clim Dynam 37(5–6):1097–1110. https://doi.org/10.1007/s00382-010-0897-9
Cook ER, Krusic PJ, Anchukaitis KJ, Buckley BM, Nakatsuka T, Sano M (2013) Tree-ring reconstructed summer temperature anomalies for temperate East Asia since 800 CE. Clim Dynam 41(11):2957–2972
Cook BI, Smerdon JE, Seager R, Coats S (2014) Global warming and 21st century drying. Clim Dynam 43(9):2607–2627
Cook ER, Seager R, Kushnir Y, Briffa KR, Büntgen U, Frank D, Krusic PJ, Tegel W, van der Schrier G, Andreu-Hayles L et al (2015) Old World megadroughts and pluvials during the Common Era. Sci Adv 1(10):e1500,561
Cook BI, Anchukaitis KJ, Touchan R, Meko DM, Cook ER (2016) Spatiotemporal drought variability in the Mediterranean over the last 900 years. J Geophys Res Atmos 121(5):2060–2074. https://doi.org/10.1002/2015JD023929
Cook BI, Mankin JS, Anchukaitis KJ (2018) Climate change and drought: From past to future. Curr Clim Change Rep 4(2):164–179
Cook ER, Kushnir Y, Smerdon JE, Williams AP, Anchukaitis KJ, Wahl ER (2019) A Euro-Mediterranean tree-ring reconstruction of the winter NAO index since 910 CE. Clim Dynam. https://doi.org/10.1007/s00382-019-04696-2
Cook ER, Solomina O, Matskovsky V, Cook BI, Agafonov L, Berdnikova A, Dolgova E, Karpukhin A, Knysh N, Kulakova M et al (2020) The European Russia drought atlas (1400–2016 ce). Clim Dynam 54(3):2317–2335
Cos J, Doblas-Reyes F, Jury M, Marcos R, Bretonnière PA, Samsó M (2022) The Mediterranean climate change hotspot in the CMIP5 and CMIP6 projections. Earth Syst Dynam 13(1):321–340
Coulthard BL, Touchan R, Anchukaitis KJ, Meko DM, Sivrikaya F (2017) Tree growth and vegetation activity at the ecosystem-scale in the eastern Mediterranean. Environ Res Lett 12(8):084,008
Cramer W, Guiot J, Fader M, Garrabou J, Gattuso JP, Iglesias A, Lange MA, Lionello P, Llasat MC, Paz S et al (2018) Climate change and interconnected risks to sustainable development in the Mediterranean. Nature Clim Change 8(11):972–980
Dai A (2011) Characteristics and trends in various forms of the Palmer Drought Severity Index during 1900–2008. J Geophys Res. https://doi.org/10.1029/2010jd015541
Dai A, Zhao T (2017) Uncertainties in historical changes and future projections of drought. Part I: estimates of historical drought changes. Clim Change 144:519–533
DeSoto L, Varino F, Andrade JP, Gouveia CM, Campelo F, Trigo RM, Nabais C (2014) Different growth sensitivity to climate of the conifer Juniperus thurifera on both sides of the Mediterranean Sea. Int J Biometeorol 58(10):2095–2109
Dorado-Liñán I, Zorita E, Martínez-Sancho E, Gea-Izquierdo G, Di Filippo A, Gutiérrez E, Levanic T, Piovesan G, Vacchiano G, Zang C et al (2017) Large-scale atmospheric circulation enhances the mediterranean east-west tree growth contrast at rear-edge deciduous forests. Agric Forest Meteorol 239:86–95
Douville H, Raghavan K, Renwick J, Allan RP, Arias PA, Barlow M, Cerezo-Mota R, Cherchi A, Gan TY, Gergis J, Jiang D, Khan A, Pokam Mba W, Rosenfeld D, Tierney J, Zolina O (2021) Water Cycle Changes. In: Masson-Delmotte V, Zhai P, Pirani A, Connors SL, Péan C, Berger S, Caud N, Chen Y, Goldfarb L, Gomis MI, Huang M, Leitzell K, Lonnoy E, Matthews JBR, Maycock TK, Waterfield T, Yelekçi O, Yu R, Zhou B (eds) Climate Change 2021: The Physical Science Basis. Contribution of Working Group I to the Sixth Assessment Report of the Intergovernmental Panel on Climate Change, Cambridge University Press, chap 8
Dünkeloh A, Jacobeit J (2003) Circulation dynamics of mediterranean precipitation variability 1948–98. Int J Climatol A 23(15):1843–1866
Esper J, Konter O, Klippel L, Krusic PJ, Büntgen U (2021) Pre-instrumental summer precipitation variability in northwestern Greece from a high-elevation Pinus heldreichii network. Int J Climatol 41(4):2828–2839
Esper J, Hartl C, Konter O, Reinig F, Römer P, Huneau F, Lebre S, Szymczak S, Bräuning A, Büntgen U (2022) Past millennium hydroclimate variability from Corsican pine tree-ring chronologies. Boreas 51(3):621–636
Esper J, Frank D, Büntgen U, Verstege A, Luterbacher J, Xoplaki E (2007) Long-term drought severity variations in Morocco. Geophysical Research Letters 34(17)
Fritts HC (1976) Tree Rings and Climate. Academic Press, New York
Galván JD, Camarero JJ, Ginzler C, Büntgen U (2014) Spatial diversity of recent trends in Mediterranean tree growth. Environ Res Lett 9(8):084,001
García-Ruiz JM, López-Moreno JI, Vicente-Serrano SM, Lasanta-Martínez T, Beguería S (2011) Mediterranean water resources in a global change scenario. Earth Sci Rev 105(3–4):121–139
Giorgi F (2006) Climate change hot-spots. Geophysical Research Letters 33(8)
Gleick PH (2014) Water, drought, climate change, and conflict in Syria. Weather Clim Soc 6(3):331–340
Griffin D, Anchukaitis KJ (2014) How unusual is the 2012–2014 california drought? Geophys Res Lett 41(24):9017–9023
Griggs C, DeGaetano A, Kuniholm P, Newton M (2007) A regional high-frequency reconstruction of May-June precipitation in

the north Aegean from oak tree rings, AD 1089–1989. Int J Climatol 27(8):1075–1089
Harris I, Osborn TJ, Jones P, Lister D (2020) Version 4 of the CRU TS monthly high-resolution gridded multivariate climate dataset. Sci Data. https://doi.org/10.1038/s41597-020-0453-3
Heinrich I, Touchan R, Liñán ID, Vos H, Helle G (2013) Winter-to-spring temperature dynamics in Turkey derived from tree rings since AD 1125. Clim Dynam 41(7–8):1685–1701. https://doi.org/10.1007/s00382-013-1702-3
Holmgren K, Gogou A, Izdebski A, Luterbacher J, Sicre MA, Xoplaki E (2016) Mediterranean Holocene climate, environment and human societies. Quat Sci Rev 136:1–4
Ide T (2018) Climate war in the Middle East? Drought, the Syrian civil war and the state of climate-conflict research. Curr Clim Change Rep 4(4):347–354
Kaiser HF (1960) The application of electronic computers to factor analysis. Educ Psychol Measure 20(1):141–151
Kelley C, Ting M, Seager R, Kushnir Y (2012) Mediterranean precipitation climatology, seasonal cycle, and trend as simulated by CMIP5. Geophys Res Lett. https://doi.org/10.1029/2012gl053416
Kelley C, Ting M, Seager R, Kushnir Y (2012) The relative contributions of radiative forcing and internal climate variability to the late 20th century winter drying of the Mediterranean region. Clim Dynam 38(9):2001–2015
Kelley CP, Mohtadi S, Cane MA, Seager R, Kushnir Y (2015) Climate change in the Fertile Crescent and implications of the recent Syrian drought. Proc Natl Acad Sci 112(11):3241–3246
King JM, Anchukaitis KJ, Tierney JE, Hakim GJ, Emile-Geay J, Zhu F, Wilson R (2021) A data assimilation approach to last millennium temperature field reconstruction using a limited high-sensitivity proxy network. J Clim. https://doi.org/10.1175/jcli-d-20-0661.1
Klippel L, Krusic PJ, Brandes R, Hartl-Meier C, Trouet V, Meko M, Esper J (2017) High-elevation inter-site differences in Mount Smolikas tree-ring width data. Dendrochronologia 44:164–173
Klippel L, Krusic PJ, Brandes R, Hartl C, Belmecheri S, Dienst M, Esper J (2018) A 1286-year hydro-climate reconstruction for the Balkan Peninsula. Boreas 47(4):1218–1229
Knutti R, Furrer R, Tebaldi C, Cermak J, Meehl GA (2010) Challenges in combining projections from multiple climate models. J Clim 23(10):2739–2758
Köse N, Akkemik Ü, Dalfes HN, Özeren MS (2011) Tree-ring reconstructions of May-June precipitation for western Anatolia. Quat Res 75(3):438–450
Köse N, Akkemik Ü, Dalfes HN, Özeren MS, Tolunay D (2012) Tree-ring growth of Pinus nigra Arn. subsp. pallasiana under different climate conditions throughout western Anatolia. Dendrochronologia 30(4):295–301
Kuglitsch FG, Toreti A, Xoplaki E, Della-Marta PM, Luterbacher J, Wanner H (2009) Homogenization of daily maximum temperature series in the mediterranean. Journal of Geophysical Research: Atmospheres 114(D15)
Kutiel H, Maheras P, Guika S (1996) Circulation and extreme rainfall conditions in the eastern mediterranean during the last century. Int J Climatol 16(1):73–92
Lelieveld J, Hadjinicolaou P, Kostopoulou E, Chenoweth J, El Maayar M, Giannakopoulos C, Hannides C, Lange M, Tanarhte M, Tyrlis E et al (2012) Climate change and impacts in the Eastern Mediterranean and the Middle East. Clim Change 114(3):667–687
Leonelli G, Coppola A, Salvatore MC, Baroni C, Battipaglia G, Gentilesca T, Ripullone F, Borghetti M, Conte E, Tognetti R et al (2017) Climate signals in a multispecies tree-ring network from central and southern Italy and reconstruction of the late summer temperatures since the early 1700s. Clim Past 13(11):1451–1471
Mariotti A, Pan Y, Zeng N, Alessandri A (2015) Long-term climate change in the Mediterranean region in the midst of decadal variability. Clim Dynam 44(5):1437–1456
Martin-Benito D, Ummenhofer CC, Köse N, Güner HT, Pederson N (2016) Tree-ring reconstructed May-June precipitation in the Caucasus since 1752 CE. Clim Dynam 47(9):3011–3027
Martin-Benito D, Anchukaitis KJ, Evans MN, Del Río M, Beeckman H, Cañellas I (2017) Effects of drought on xylem anatomy and water-use efficiency of two co-occurring pine species. Forests 8(9):332
Martin-Benito D, Pederson N, Köse N, Doğan M, Bugmann H, Mosulishvili M, Bigler C (2018) Pervasive effects of drought on tree growth across a wide climatic gradient in the temperate forests of the Caucasus. Global Ecoly Biogeogr 27(11):1314–1325
McPartland M, George SS, Pederson GT, Anchukaitis KJ (2020) Does signal-free detrending increase chronology coherence in large tree-ring networks? Dendrochronologia 63(125):755. https://doi.org/10.1016/j.dendro.2020.125755
Meko D (1997) Dendroclimatic Reconstruction with Time Varying Predictor Subsets of Tree Indices. J Clim 10:687–696
Meko DM, Baisan CH (2001) Pilot study of latewood-width of conifers as an indicator of variability of summer rainfall in the North American monsoon region. Int J Climatol 21(6):697–708
Meko D, Cook ER, Stahle DW, Stockton CW, Hughes MK (1993) Spatial patterns of tree-growth anomalies in the united states and southeastern canada. J Clim 6(9):1773–1786
Melvin T, Briffa K (2008) A 'signal-free' approach to dendroclimatic standardisation. Dendrochronologia 26(2):71–86
Monahan AH, Fyfe JC, Ambaum MH, Stephenson DB, North GR (2009) Empirical orthogonal functions: The medium is the message. J Clim 22(24):6501–6514
Nicault A, Alleaume S, Brewer S, Carrer M, Nola P, Guiot J (2008) Mediterranean drought fluctuation during the last 500 years based on tree-ring data. Clim Dynam 31(2):227–245
Pacheco A, Camarero JJ, Carrer M (2016) Linking wood anatomy and xylogenesis allows pinpointing of climate and drought influences on growth of coexisting conifers in continental Mediterranean climate. Tree Physiol 36(4):502–512
Palmer WC (1965) Meteorological drought. Tech. rep., U.S. Weather Bureau Research Paper 45
Palmer JG, Cook ER, Turney CS, Allen K, Fenwick P, Cook BI, O'Donnell A, Lough J, Grierson P, Baker P (2015) Drought variability in the eastern Australia and New Zealand summer drought atlas (ANZDA, CE 1500–2012) modulated by the Interdecadal Pacific Oscillation. Environ Res Lett 10(12):124,002
Piermattei A, Crivellaro A, Krusic PJ, Esper J, Vítek P, Oppenheimer C, Felhofer M, Gierlinger N, Reinig F, Urban O et al (2020) A millennium-long 'Blue Ring'chronology from the Spanish Pyrenees reveals severe ephemeral summer cooling after volcanic eruptions. Environ Res Lett 15(12):124,016
Rao MP, Cook BI, Cook ER, D'Arrigo RD, Krusic PJ, Anchukaitis KJ, LeGrande AN, Buckley BM, Davi NK, Leland C et al (2017) European and Mediterranean hydroclimate responses to tropical volcanic forcing over the last millennium. Geophys Res Lett 44(10):5104–5112
Seager R, Osborn TJ, Kushnir Y, Simpson IR, Nakamura J, Liu H (2019) Climate Variability and Change of Mediterranean-Type Climates. J Clim 32(10):2887–2915. https://doi.org/10.1175/jcli-d-18-0472.1
Seager R, Liu H, Kushnir Y, Osborn TJ, Simpson IR, Kelley CR, Nakamura J (2020) Mechanisms of Winter precipitation variability in the European-Mediterranean region associated with the North Atlantic oscillation. J Clim 33(16):7179–7196
Seim A, Treydte K, Trouet V, Frank D, Fonti P, Tegel W, Panayotov M, Fernández-Donado L, Krusic P, Büntgen U (2015) Climate

sensitivity of mediterranean pine growth reveals distinct east-west dipole. Int J Climatol 35(9):2503–2513
Selby J, Dahi OS, Fröhlich C, Hulme M (2017) Climate change and the Syrian civil war revisited. Polit Geogr 60:232–244
Smerdon JE, Cook BI, Cook ER, Seager R (2015) Bridging Past and Future Climate across Paleoclimatic Reconstructions, Observations, and Models: A Hydroclimate Case Study. J Clim 28(8):3212–3231. https://doi.org/10.1175/jcli-d-14-00417.1
Snee RD (1977) Validation of regression models: methods and examples. Technometrics 19(4):415–428
Steiger NJ, Smerdon JE, Cook ER, Cook BI (2018) A reconstruction of global hydroclimate and dynamical variables over the Common Era. Sci Data. https://doi.org/10.1038/sdata.2018.86
Stevenson S, Coats S, Touma D, Cole J, Lehner F, Fasullo J, Otto-Bliesner B (2022) Twenty-first century hydroclimate: A continually changing baseline, with more frequent extremes. Proc Natl Acad Sci. https://doi.org/10.1073/pnas.2108124119
Stokes M, Smiley T (1968) An Introduction to Tree-Ring Dating. University of Chicago Press, Chicago, IL
Suárez-Moreno R, Kushnir Y, Seager R (2022) Observational analysis of decadal and long-term hydroclimate drivers in the Mediterranean region: role of the ocean-atmosphere system and anthropogenic forcing. Clim Dynam 58(7):2079–2107
Tanarhte M, Hadjinicolaou P, Lelieveld J (2012) Intercomparison of temperature and precipitation data sets based on observations in the mediterranean and the middle east. Journal of Geophysical Research: Atmospheres 117(D12)
Tejedor E, de Luis M, Cuadrat JM, Esper J, Saz MÁ (2016) Tree-ring-based drought reconstruction in the Iberian Range (east of Spain) since 1694. Int J Biometeorol 60(3):361–372
Tejedor E, Saz M, Esper J, Cuadrat J, De Luis M (2017) Summer drought reconstruction in northeastern Spain inferred from a tree ring latewood network since 1734. Geophys Res Lett 44(16):8492–8500
Touchan R, Hughes MK (1999) Dendrochronology in Jordan. J Arid Environ 42(4):291–303
Touchan R, Meko D, Hughes MK (1999) A 396-year reconstruction of precipitation in southern Jordan. J Am Water Resources Assoc 35(1):49–59
Touchan R, Meko D, Hughes MK (1999) A 396-year Reconstruction of Precipitation in Southern Jordan. JAWRA 35(1):49–59
Touchan R, Garfin GM, Meko DM, Funkhouser G, Erkan N, Hughes MK, Wallin BS (2003) Preliminary reconstructions of spring precipitation in southwestern Turkey from tree-ring width. Int J Climatol 23(2):157–171
Touchan R, Funkhouser G, Hughes MK, Erkan N (2005) Standardized Precipitation Index Reconstructed from Turkish Tree-Ring Widths. Clim Change 72(3):339–353. https://doi.org/10.1007/s10584-005-5358-9
Touchan R, Xoplaki E, Funkhouser G, Luterbacher J, Hughes MK, Erkan N, Akkemik U, Stephan J (2005) Reconstructions of spring/summer precipitation for the Eastern Mediterranean from tree-ring widths and its connection to large-scale atmospheric circulation. Clim Dynam 25:75–98
Touchan R, Akkemik U, Hughes MK, Erkan N (2007) May-June precipitation reconstruction of southwestern Anatolia, Turkey during the last 900 years from tree rings. Quat Res 68(2):196–202. https://doi.org/10.1016/j.yqres.2007.07.001
Touchan R, Anchukaitis KJ, Meko DM, Attalah S, Baisan C, Aloui A (2008) Long term context for recent drought in northwestern Africa. Geophys Res Lett 35(13):L13,705
Touchan R, Meko DM, Aloui A (2008) Precipitation reconstruction for northwestern Tunisia from tree rings. J Arid Environ 72:1887–1896
Touchan R, Anchukaitis KJ, Meko DM, Sabir M, Attalah S, Aloui A (2011) Spatiotemporal drought variability in northwestern Africa over the last nine centuries. Clim Dynam 37(1–2):237–252. https://doi.org/10.1007/s00382-010-0804-4
Touchan R, Shishov V, Meko D, Nouiri I, Grachev A (2012) Process based model sheds light on climate sensitivity of Mediterranean tree-ring width. Biogeosciences 9(3):965–972
Touchan R, Anchukaitis KJ, Shishov VV, Sivrikaya F, Attieh J, Ketmen M, Stephan J, Mitsopoulos I, Christou A, Meko DM (2014) Spatial Patterns of eastern Mediterranean climate influence on tree growth. Holocene 24(4):381–392. https://doi.org/10.1177/0959683613518594
Touchan R, Christou AK, Meko DM (2014) Six centuries of May-July precipitation in Cyprus from tree rings. Clim Dynam. https://doi.org/10.1007/s00382-014-2104-x
Touchan R, Meko DM, Anchukaitis KJ (2014) Dendroclimatology in the eastern mediterranean. Radiocarbon 56(4):S61–S68
Touchan R, Shishov VV, Tychkov II, Sivrikaya F, Attieh J, Ketmen M, Stephan J, Mitsopoulos I, Christou A, Meko DM (2016) Elevation-layered dendroclimatic signal in eastern Mediterranean tree rings. Environ Res Lett 11(4):044,020
Touchan R, Anchukaitis KJ, Meko DM, Kerchouche D, Slimani S, Ilmen R, Hasnaoui F, Guibal F, Julio Camarero J, Sánchez-Salguero R et al (2017) Climate controls on tree growth in the Western Mediterranean. Holocene 27(10):1429–1442
Tramblay Y, Koutroulis A, Samaniego L, Vicente-Serrano SM, Volaire F, Boone A, Le Page M, Llasat MC, Albergel C, Burak S et al (2020) Challenges for drought assessment in the Mediterranean region under future climate scenarios. Earth Sci Rev 210(103):348
Trenberth KE, Dai A, Van Der Schrier G, Jones PD, Barichivich J, Briffa KR, Sheffield J (2014) Global warming and changes in drought. Nature Clim Change 4(1):17–22
Tuel A, Eltahir EA (2020) Why is the Mediterranean a climate change hot spot? J Clim 33(14):5829–5843
van der Schrier G, Barichivich J, Briffa KR, Jones PD (2013) A scPDSI-based global data set of dry and wet spells for 1901–2009. J Geophys Res. https://doi.org/10.1002/jgrd.50355
Vicente-Serrano SM, Lopez-Moreno JI, Beguería S, Lorenzo-Lacruz J, Sanchez-Lorenzo A, García-Ruiz JM, Azorin-Molina C, Morán-Tejeda E, Revuelto J, Trigo R et al (2014) Evidence of increasing drought severity caused by temperature rise in southern Europe. Environ Res Lett 9(4):044,001
Vicente-Serrano SM, Van der Schrier G, Beguería S, Azorin-Molina C, Lopez-Moreno JI (2015) Contribution of precipitation and reference evapotranspiration to drought indices under different climates. J Hydrol 526:42–54
Vicente-Serrano SM, McVicar TR, Miralles DG, Yang Y, Tomas-Burguera M (2020) Unraveling the influence of atmospheric evaporative demand on drought and its response to climate change. Wiley Interdisciplinary Reviews. Clim Change 11(2):e632
Wells N, Goddard S, Hayes MJ (2004) A self-calibrating Palmer drought severity index. J Clim 17(12):2335–2351
Williams AP, Cook ER, Smerdon JE, Cook BI, Abatzoglou JT, Bolles K, Baek SH, Badger AM, Livneh B (2020) Large contribution from anthropogenic warming to an emerging North American megadrought. Science 368(6488):314–318
Williams A, Anchukaitis K, Woodhouse C, Meko D, Cook B, Bolles K, Cook E (2021) Tree rings and observations suggest no stable cycles in Sierra Nevada cool-season precipitation. Water Resour Res 57(3):599
Xoplaki E, González-Rouco J, Luterbacher J, Wanner H (2004) Wet season mediterranean precipitation variability: influence of large-scale dynamics and trends. Clim Dynam 23:63–78
Xoplaki E, Luterbacher J, Wagner S, Zorita E, Fleitmann D, Preiser-Kapeller J, Sargent AM, White S, Toreti A, Haldon JF et al (2018) Modelling climate and societal resilience in the

Eastern Mediterranean in the last millennium. Human Ecol 46(3):363–379

Zhang X, Aguilar E, Sensoy S, Melkonyan H, Tagiyeva U, Ahmed N, Kutaladze N, Rahimzadeh F, Taghipour A, Hantosh T et al (2005) Trends in middle east climate extreme indices from 1950 to 2003. Journal of Geophysical Research: Atmospheres 110(D22)

Authors and Affiliations

Kevin J. Anchukaitis[1] · Ramzi Touchan[2] · David M. Meko[2] · Dalila Kherchouche[3] · Said Slimani[4] · Fatih Sivrikaya[5] · Rachid Ilmen[6] · Ioannis Mitsopoulos[7] · Jean Stephan[8] · Jihad Attieh[9] · Foued Hasnaoui[10] · J. Julio Camarero[11] · Raúl Sánchez-Salguero[11,12] · Frederic Guibal[13] · Alma Piermattei[14,18] · Andreas Christou[15] · Jordan Krcmaric[16] · Benjamin I. Cook[17]

✉ Kevin J. Anchukaitis
kanchukaitis@arizona.edu

[1] School of Geography, Development and Environment and Laboratory of Tree-Ring Research, University of Arizona, Tucson, AZ, US

[2] Laboratory of Tree-Ring Research, University of Arizona, Tucson, AZ, USA

[3] Institute of Veterinary and Agronomy Sciences, University of Batna 1, Batna, Algeria

[4] Department of Ecology, Faculty of Biological and Agricultural Sciences, Mouloud Mammeri University of Tizi Ouzou, Tizi Ouzou, Algeria

[5] Department of Forest Management, Faculty of Forestry, Kastamonu University, 37150 Kastamonu, Türkiye

[6] Department of Hydraulic, Environment and Climate (HEC), Hassania School of Public Works (EHTP), km 7, Road of El Jadida, P. O. Box 8108 Oasis-Casablanca, Morocco

[7] Natural Environment and Climate Change Agency (NECCA), L.Mesogeion 207, 11525 Athens, Greece

[8] Biodiversity Conservation and Management of Natural Resources, Faculty of Science Fanar, Lebanese University, Beirut, Lebanon

[9] Department of Biology, Faculty of Arts and Sciences, University of Balamand, Balamand, Lebanon

[10] Institute of Sylvo-pastoral of Tabaraka, Tabarka, Tunisia

[11] Pyrenean Institute of Ecology, IPE-CSIC, Avda. Montañana 1005, 50059 Zaragoza, Spain

[12] Department of Physical, Chemical and Natural Systems, Univ. Pablo de Olavide, Ctra. Utrera km. 1, 41013 Seville, Spain

[13] Mediterranean Institute for Biodiversity and Ecology, Aix Marseille Univ, Avignon University, CNRS, IRD, Aix-en-Provence, France

[14] Department of Agricultural, Forest and Food Sciences, University of Torino, Largo Braccini 2, 10095 Grugliasco, Italy

[15] Department of Forests, 1414 Nicosia, Cyprus

[16] National Geodetic Survey, National Oceanic and Atmospheric Administration (NOAA), Silver Spring, Maryland, US

[17] NASA Goddard Institute for Space Studies, New York, New York, US

[18] Forest Biometrics Laboratory, Faculty of Forestry, "Stefan cel Mare" University of Suceava, Str. Universitatii 13, Suceava, Romania